© 2021. Published by The Company of Biologists Ltd | Development (2021) 148, dev199426. doi:10.1242/dev.199426

RESEARCH ARTICLE

Maternal RNF114-mediated target substrate degradation regulates zygotic genome activation in mouse embryos

Shuai Zhou[1,3,*], Yueshuai Guo[1,*], Haifeng Sun[1,*], Lu Liu[1], Liping Yao[1], Chao Liu[2], Yuanlin He[1], Shanren Cao[3], Cheng Zhou[1], Mingrui Li[1], Yumeng Cao[1], Congjing Wang[1], Qianneng Lu[1], Wei Li[2,‡], Xuejiang Guo[1,‡] and Ran Huo[1,‡]

ABSTRACT

Zygotic genomic activation (ZGA) is a landmark event in the maternal-to-zygotic transition (MZT), and the regulation of ZGA by maternal factors remains to be elucidated. In this study, the depletion of maternal ring finger protein 114 (RNF114), a ubiquitin E3 ligase, led to developmental arrest of two-cell mouse embryos. Using immunofluorescence and transcriptome analysis, RNF114 was proven to play a crucial role in major ZGA. To study the underlying mechanism, we performed protein profiling in mature oocytes and found a potential substrate for RNF114, chromobox 5 (CBX5), ubiquitylation and degradation of which was regulated by RNF114. The overexpression of CBX5 prevented embryonic development and impeded major ZGA. Furthermore, TAB1 was abnormally accumulated in mutant two-cell embryos, which was consistent with the result of *in vitro* knockdown of *Rnf114*. Knockdown of *Cbx5* or *Tab1* in maternal RNF114-depleted embryos partially rescued developmental arrest and the defect of major ZGA. In summary, our study reveals that maternal RNF114 plays a precise role in degrading some important substrates during the MZT, the misregulation of which may impede the appropriate activation of major ZGA in mouse embryos.

KEY WORDS: Maternal RNF114, Zygotic genomic activation, Preimplantation embryo development, Ubiquitin degradation, CBX5, TAB1

INTRODUCTION

The maternal-to-zygotic transition (MZT), which occurs at the initial stage of embryogenesis and involves a variety of biological events, transforms highly differentiated oocytes into totipotent embryos in mammals (Vastenhouw et al., 2019). The degradation of maternal factors and zygotic genome activation (ZGA) are the two vital events of MZT. Maternal RNAs and proteins accumulated during oocyte maturation are rapidly degraded once their duties have been accomplished after fertilization (Esencan et al., 2019; Toralova et al., 2020). Major ZGA, which occurs at the two-cell stage in mouse embryos, takes embryos from the state of little transcription to the condition where thousands of genes are actively transcribed (Ko, 2016). Given that the parental genomes show a quiescent state before ZGA, it is believed that the initial stage of development is mainly controlled by maternal factors (Kim and Lee, 2014). For example, maternal deletion of *Imp2* (also known as *Igf2bp2*) and *Mater* (*Nlrp5*) causes early embryo arrest at the two-cell stage owing to the loss of the ability to regulate and activate genes that are involved in major ZGA (Liu et al., 2019; Tong et al., 2000). However, the abnormal accumulation of maternal factors leads to the retardation of embryonic development. Embryos derived from *Btg4*$^{-/-}$ females or following knockdown of *Ago2* arrest at the one- or two-cell stage, resulting mainly from the deficient clearance of maternal mRNAs during MZT (Lykke-Andersen et al., 2008; Wu and Dean, 2016). Thus, there is a balance between degradation and retention for maternal factors to regulate subsequent development at embryogenesis (Sha et al., 2019). However, the mechanism by which maternal factors regulate the degradation of RNAs and proteins to drive the activation of major ZGA has not been elucidated until now.

Ring finger protein 114 (RNF114) contains two C2H2 zinc-finger domains and one RING-finger domain (Giannini et al., 2008). Some relevant studies have reported that RNF114 protein usually functions as an E3 ligase in the ubiquitin-proteasome system and plays an important role in basic cellular processes in different types of cells (Han et al., 2013; Lin et al., 2018, 2017; Yang et al., 2014). Meanwhile, RNF114 was found to be predominantly expressed in mouse oocytes but decreased gradually after fertilization (Wang et al., 2010; Zhang et al., 2009). A previous study demonstrated that the knockdown of *Rnf114* in zygotes significantly influenced preimplantation development, mainly affecting the degradation of potential substrate protein TAB1 (Yang et al., 2017). However, this strategy did not reflect the role of RNF114 as a maternal protein in mouse embryonic development.

In this study, we constructed an *Rnf114* mutant mouse strain by gene editing to further investigate the function of maternal RNF114 in MZT. We found that edited female mice were completely infertile, whereas male mice were unaffected. Although no abnormalities were found in ovulation, oocyte morphology or fertilization potential, the zygotes derived from *Rnf114*-mutant oocytes led to developmental arrest at the two-cell stage, with major ZGA failing to fully activate. Through proteome detection, we found a potential substrate of RNF114 in mutant oocytes, chromobox 5 (CBX5; also named heterochromatin protein 1 alpha, HP1α), the abnormal overexpression of which resulted in decreased major ZGA and embryonic developmental disorder. Moreover, we also found that TAB1, a proven substrate, was increased in two-cell embryos with the deletion of maternal RNF114. A few embryos could reach the

[1]State Key Laboratory of Reproductive Medicine, Department of Histology and Embryology, The Affiliated Suzhou Hospital of Nanjing Medical University, Suzhou Municipal Hospital, Gusu School, Nanjing Medical University, Nanjing 211166, China. [2]State Key Laboratory of Reproductive Biology, Institute of Zoology, Chinese Academy of Sciences, Beijing 100101, China. [3]Department of Reproductive Medicine, Women's Hospital of Nanjing Medical University, Nanjing Maternity and Child Health Care Hospital, Nanjing 210004, China.
*These authors contributed equally to this work

‡Authors for correspondence (huoran@njmu.edu.cn; guo_xuejiang@njmu.edu.cn; leways@ioz.ac.cn)

W.L., 0000-0002-6235-0749; R.H., 0000-0001-5166-127X

Handling Editor: Maria Elena Torres-Padilla
Received 17 January 2021; Accepted 27 May 2021

Development (2021) 148, dev199426. doi:10.1242/dev.199426

blastocyst stage and the level of some major ZGA genes increased significantly when *Cbx5* or *Tab1* were knocked down in mutant zygotes. Our study reveals that RNF114, as a maternal factor, plays an important role in degrading specific substrates during MZT, and thus participates in regulation of major ZGA.

RESULTS

Loss of maternal RNF114 arrests early embryonic development beyond the two-cell stage

RNF114 protein is notably expressed in mouse oocytes, and *in vitro* knockdown of *Rnf114* impaired early embryonic development (Yang et al., 2017). To examine the *in vivo* function of maternal RNF114, we generated a mouse strain in which *Rnf114* had 81 bp deleted at exon 2, resulting in the destruction of the RING domain in RNF114 (Fig. S1A). According to the gene editing strategy, we designed three pairs of primers: P1, across the deletion region; P2, forward primer inside the deletion region; P3, behind the deletion region; this was done to verify editing efficiency (Fig. S1B). The *Rnf114* mutation was confirmed by RT-PCR of P2 in metaphase II (MII) oocytes isolated from control and mutant females (Fig. S1C). Although only partially missing, the overall levels of *Rnf114* mRNA in mutant oocytes decreased significantly (Fig. S1D). Moreover, immunoblot staining confirmed the greatly decreased level of RNF114 protein in mutant ovaries (Fig. S1E). Thus, we named the control group $Rnf114^{+/-}$ and the mutant group $Rnf114^{-/-}$. $Rnf114^{-/-}$ females were completely infertile when mated with wild-type (WT) males (Fig. 1A). However, when $Rnf114^{-/-}$ male mice were mated with one or two $Rnf114^{+/-}$ female mice to obtain homozygous offspring, the average number of pups was 8.5 in each litter (n=5), which indicated the fertility of $Rnf114^{-/-}$ male mice was not affected. To investigate the potential defect in female germ cell development, we prepared haematoxylin and eosin (H&E)-stained sections of ovaries from the $Rnf114^{+/-}$ and $Rnf114^{-/-}$ females. There were no histological defects in $Rnf114^{-/-}$ ovaries upon analysing the different stages of follicles and counting the total follicle numbers (Fig. S2A,B). Moreover, the number of oocytes from superovulated $Rnf114^{-/-}$ females was comparative with that of $Rnf114^{+/-}$ females (Fig. S2C), and immunofluorescent staining for α-tubulin and DNA showed normal spindles in the mutant MII oocytes (Fig. S2D,E). We subsequently combined $Rnf114^{-/-}$ oocytes with WT sperm by *in vitro* fertilization (IVF) to obtain $Rnf114^{m-z+}$ embryos, indicating maternal loss (m−) but zygotic presence (z+) of the RNF114 protein (Fig. 1B). $Rnf114^{m-z+}$ embryos almost arrested at the two-cell stage, compared with $Rnf114^{m+z+}$ embryos (Fig. 1C,D). These results suggested that maternal RNF114 was essential for mouse preimplantation development.

Maternal RNF114 depletion inhibits major ZGA

As major ZGA is one of the crucial cellular events for preimplantation development, taking place at the two-cell stage in mouse embryos, we explored whether major ZGA might be impaired in mutant embryos by following several strategies. The incorporation of the uridine analogue ethynyl uridine (EU) (Jao and Salic, 2008), measuring newly synthesized transcripts, revealed a conspicuously lower detectable intensity in $Rnf114^{m-z+}$ two-cell embryos than in $Rnf114^{m+z+}$ two-cell embryos (Fig. 2A,B). The phosphorylation status of Ser2 or Ser5 on the C-terminal domain of RNA Polymerase II is also an excellent measure of transcription initiation, as RNA Pol II requires these serine phosphorylation events to be part of the initiation and elongation complex, respectively (Egloff and Murphy, 2008). A significant reduction in Pol II Ser-2p (Fig. 2C,D) and Pol II Ser-5p (Fig. 2E,F) staining in $Rnf114^{m-z+}$ embryos demonstrated that RNA Pol II is not engaged in transcription at the time of ZGA in mutant embryos. Moreover, SIRT1, which has been proven to be a product of early zygotic transcription (Nagaraj et al., 2017), decreased significantly in the $Rnf114^{m-z+}$ embryos (Fig. 2G,H). Taken together, we concluded that the absence of maternal RNF114 blocked major ZGA during MZT.

To further explore the disordered transcription caused by the absence of RNF114, we performed oocyte and embryo transcriptome profiling. According to the time course of embryonic development, *Rnf114*-deleted MII oocytes and maternal *Rnf114*-depleted one-cell and two-cell embryos were collected (mutant group). Strain-matched $Rnf114^{+/-}$ oocytes and $Rnf114^{m+z+}$ embryos served as a control group. Each stage had four to five replicates, and 15-20 cells were harvested in every replicate sample (Fig. 3A; Table S1). The number of raw and mapped reads in RNA sequencing was similar between the

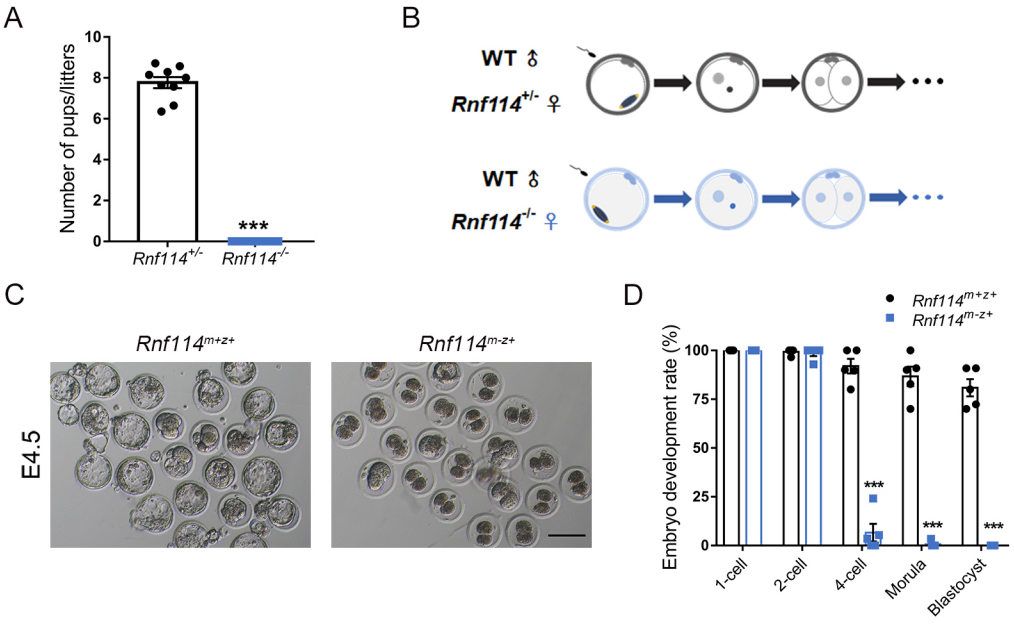

Fig. 1. Maternal *Rnf114* deletion arrests early embryonic development beyond the two-cell stage. (A) The average number of pups per litter from $Rnf114^{+/-}$ and $Rnf114^{-/-}$ females mating with normal fertile males over six months. n=9, total of 9-13 females/group. (B) Schematic of obtaining the $Rnf114^{m+z+}$ embryo (grey) and $Rnf114^{m-z+}$ embryo (blue) by IVF. (C) Representative differential interference contrast images of $Rnf114^{m+z+}$ and $Rnf114^{m-z+}$ embryos at 4.5 days (E4.5). Scale bars: 100 µm. (D) Percentage of embryos to reach the various preimplantation embryo stages from $Rnf114^{m+z+}$ and $Rnf114^{m-z+}$ one-cell embryos. n=5, total of 85-143 embryos/group. Data are mean±s.e.m. ***P<0.001 (unpaired two-tailed t-test).

Development (2021) 148, dev199426. doi:10.1242/dev.199426

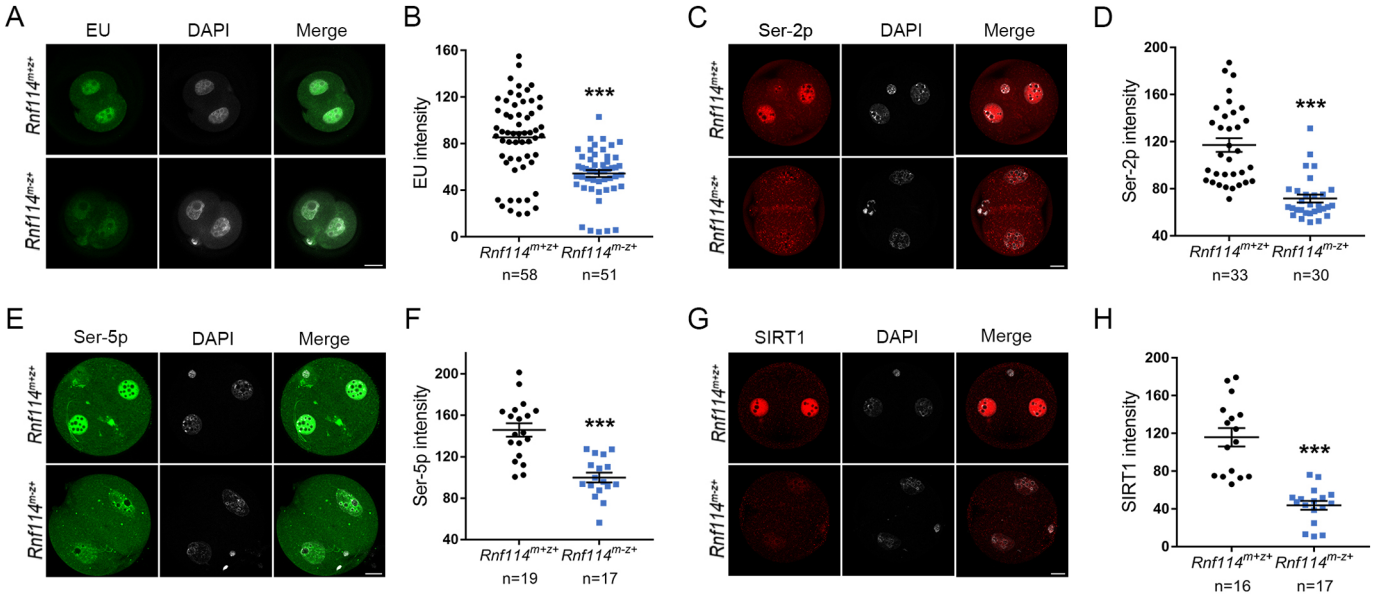

Fig. 2. Loss of maternal *Rnf114* inhibits major ZGA. (A) EU staining as an indicator of transcription levels. (B) Quantification of EU staining in $Rnf114^{m+z+}$ and $Rnf114^{m-z+}$ two-cell embryos. (C) Phosphorylation levels of serine moieties at position 2 of Pol II for $Rnf114^{m+z+}$ and $Rnf114^{m-z+}$ two-cell embryos. (D) Quantification of Ser-2p staining. (E) Phosphorylation levels of serine moieties at position 5 in Pol II. (F) Quantification of Ser-5p staining in $Rnf114^{m+z+}$ and $Rnf114^{m-z+}$ embryos. (G) Representative images of SIRT1 staining showing the decreased level of transcription in $Rnf114^{m-z+}$ two-cell embryos. (H) Quantification of SIRT1 staining in $Rnf114^{m+z+}$ and $Rnf114^{m-z+}$ embryos. Error bars represent s.e.m. ***P<0.001 (unpaired two-tailed t-test). Scale bars: 20 µm.

control and mutant group during different cell periods (Fig. S3A). In addition, the total genes detected in the same period had no significant difference between the two groups, with fragments per kilobase million (FPKM) >1 as the gene expression threshold (Fig. S3B). Principal component analysis (PCA) showed that the separation in two-cell embryos was the largest in principal component 1 (PC1) and PC2, representing a wide difference between the control and mutant group (Fig. 3B). In differential expression gene (DEG) analysis (fold change>2, adjusted P-value<0.05; Table S2), we found that only three genes overlapped across all stages, including *Rnf114*, expression of which was reduced significantly in the mutant group (Fig. S3C,D). As only 13 DEGs were detected in the one-cell stage (Fig. 3C), we assessed the level of minor ZGA, which proceeds in zygotes (Abe et al., 2018). There was no difference in the EU level and the staining of Pol II Ser-2p and Ser-5p in $Rnf114^{m-z+}$ zygotes, compared with the control embryos (Fig. S4A-D). These results suggested the level of transcription at minor ZGA was essentially normal in $Rnf114^{m-z+}$ zygotes.

The number of DEGs detected in the two-cell embryos was over 6000 (Fig. 3C; Table S2). This meant the abnormalities mainly occurred at the two-cell stage. Then, the DEGs were compared against a public database of early mouse embryonic transcriptomes (a database of transcriptome in mouse early embryos, DBTMEE) (Park et al., 2015), where genes were categorized by specific expression pattern (Huang et al., 2017). We observed a striking enrichment of maternal transcript clusters (maternal RNA and minor ZGA) and a deficiency of zygotic transcript clusters (major ZGA and two-cell transient activation) in $Rnf114^{m-z+}$ two-cell embryos (Fig. 3D). Furthermore, time-series clustering of gene expression showed that the two-cell DEGs belonging to the maternal RNA cluster in the $Rnf114^{m-z+}$ embryos did not decrease to the same level as in the control samples. On the other hand, the overlapping genes between the two-cell embryo DEGs and the major ZGA cluster were significantly inactive in the mutant embryos (Fig. 3E). In addition, the expression differences were validated by quantitative RT-PCR analyses, which were performed on the samples independent from the transcriptome. Genes pertaining to the cluster of maternal RNA (*Npm2*, *Uchl1*, *Zar1* and *Zfp57*) and minor ZGA (*Msx1*, *Wee2*, *Zfp352*, *Zscan4c* and *Zscan4d*) showed higher expression, whereas those subjected to the major ZGA cluster (*Eif1a*, *Kdm5a*, *Nop16*, *Ppp1r15b* and *Sirt1*) were expressed at lower levels in the $Rnf114^{m-z+}$ two-cell embryos (Fig. S3E). Gene ontology (GO) analysis of the upregulated genes revealed an enrichment of negative regulation of transcription and multicellular organism development, and downregulated genes were enriched for ribosome biogenesis, RNA processing and transcription (Fig. 3F; Table S3). In summary, RNA sequencing analysis suggested that embryos that lost maternal RNF114 suffered serious impairment in MZT, as judged by the abnormal accumulation of maternal transcripts and failure to activate zygotic transcripts.

RNF114 depletion causes abnormal accumulation of CBX3 and CBX5 in oocytes

Because RNF114 is a highly expressed E3 ubiquitin ligase in oocytes, the deletion of RNF114 may lead to abnormal protein metabolism during oocyte maturation, thus affecting embryonic development. Moreover, to avoid the influence of paternal origin factors in the mutant embryos, we detected the proteome of the MII oocytes derived from $Rnf114^{+/-}$ and $Rnf114^{-/-}$ females. There were three replicates in each of the two groups for quantitative proteomics analysis. A total of 5451 proteins were identified in the proteomics analysis from $Rnf114^{+/-}$ and $Rnf114^{-/-}$ oocytes. Quantitative analysis of the proteomics data revealed that 91 proteins were upregulated and 45 proteins were downregulated (fold change>1.2, P <0.05, unpaired two-tailed t-test), and RNF114 was the most significantly downregulated protein in $Rnf114^{-/-}$ oocytes, compared with $Rnf114^{+/-}$ oocytes (Fig. 4A; Table S4). From the analysis of the interaction network of differentially expressed proteins, we found that two sets were enriched, one of which gathered histone subunits and chromatin binding proteins (Fig. 4B).

Development (2021) 148, dev199426. doi:10.1242/dev.199426

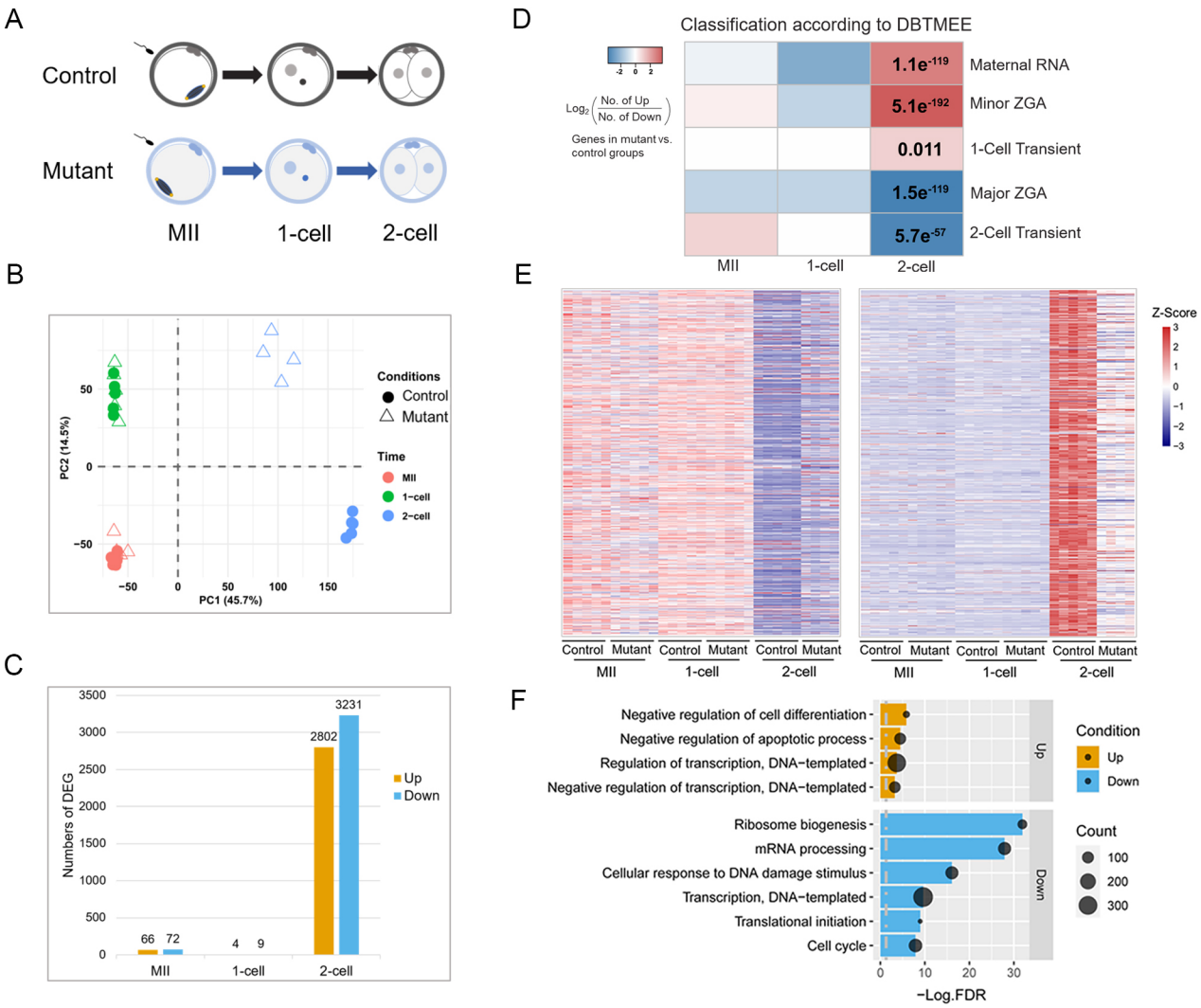

Fig. 3. Maternal RNA114 deletion leads to abnormal accumulation of maternal transcripts and major ZGA inactivation. (A) Schematic of collecting samples from different periods in control and mutant group. (B) Score plot of the first two principal components for all groups using specific developmental time points. (C) Quantification of the number of differentially expressed genes (DEGs) in each group at different time points (a fold change >2 and an adjusted *P*-value<0.05). (D) Heatmap representing the $\log_2$ ratio of the number of upregulated genes to downregulated genes in the mutant group compared with the control group at each time point, pertaining to the known cluster of DBTMEE. *P*-value<0.05 was displayed in the heatmap (Fisher's exact test). (E) Time-series clustering of DEGs derived from two-cell embryos overlapping with the maternal RNA cluster (left) and major ZGA cluster from the DBTMEE database. (F) Highly significant GO categories of upregulated and downregulated genes in two-cell embryos. The chart represents the $\log_{10}$ *P*-value, and the size of the circle indicates the number of genes in the category. The grey dotted line indicates FDR=0.05.

Furthermore, GO analysis of the differentially expressed proteins revealed that the terms related to DNA and chromatin ('nuclear heterochromatin', 'site of DNA damage', etc.) were enriched in cellular components (CC) and molecular functions (MF), although not gathered in biological processes (BP) (Fig. 4C). We then noticed the proteins chromobox homologue 3 and 5 [CBX3 and CBX5, also named heterochromatin protein 1 (HP1) isoforms HP1γ and HP1α], associated with the GO terms of DNA and chromatin, were accumulated in the *Rnf114*$^{-/-}$ oocytes (Fig. 4A; Table S5). To investigate the potential relationships between RNF114 and CBX proteins, the proteomic results were first validated by independent analyses. Western blot analysis of CBX3 and CBX5 from the *Rnf114*$^{-/-}$ MII oocytes confirmed their abnormal accumulation (Fig. 4D,E).

To investigate whether RNF114 is a ubiquitin ligase for CBX proteins, we expressed *Cbx*-Flag and HA-*Ub* in 293T cells and co-transfected them with *Rnf114*-Myc vector, followed by proteasome inhibitor MG132 treatment. The ubiquitylation level of CBX3 was not changed in the presence of RNF114 in the immunoprecipitation pulled down by anti-Flag beads (Fig. 5A). However, we observed an increased ubiquitylation of CBX5 upon RNF114 expression (Fig. 5B). As expected, increasing the expression of RNF114 resulted in a decrease in the expression of CBX5 but not CBX3 in the condition without MG132 (Fig. 5C,D). In general, loss of RNF114 caused aberrant enrichment of CBX3 and CBX5 in mouse oocytes. Further study indicated that RNF114 mediated the ubiquitylation and degradation of CBX5 but not CBX3.

Embryos overexpressing CBX5 undergo defective major ZGA

CBX proteins are not only structural components of heterochromatin but also play a role in DNA replication, cell cycle and gene expression (Kumar and Kono, 2020; Maison and Almouzni, 2004). We examined the expression patterns of CBX3 and CBX5 in normal oocytes and embryos (Fig. S5A,B). The results

Development (2021) 148, dev199426. doi:10.1242/dev.199426

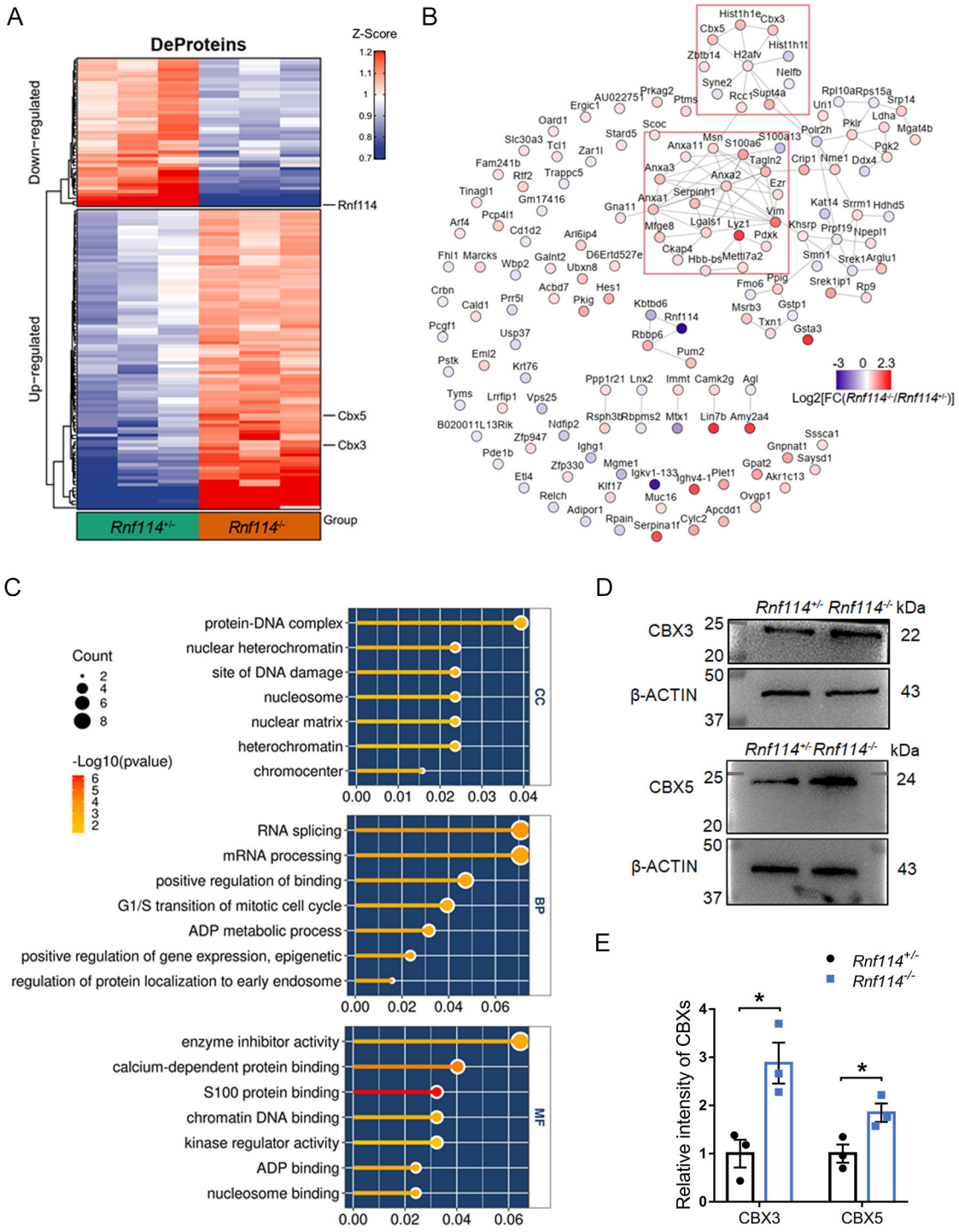

Fig. 4. RNF114 depletion causes an accumulation of CBX3 and CBX5 in oocytes. (A) Unsupervised hierarchical clustering of differential expression proteins in *Rnf114*$^{+/-}$ and *Rnf114*$^{-/-}$ oocytes (fold change>1.2; *P*-value<0.05). *n*=3, independent replicates. (B) Protein interaction network analysis on differential expression proteins. The colour of the dot indicates the change in protein expression and the red boxes represent protein clusters. (C) Highly significant GO analysis on differential proteins in *Rnf114*$^{-/-}$ oocytes. The colour of the line represents the $\log_{10}$ *P*-value, and the size of the circle indicates the number of genes in the category. (D) Western blot of CBX3 and CBX5 in the control and RNF114-depleted oocytes. β-Actin was used as a loading control. (E) Quantitative analysis of CBX3 and CBX5 protein levels from D. *n*=3, independent replicates. Data are mean±s.e.m. **P*<0.05 (the unpaired two-tailed *t*-test).

showed that the expression level of CBX3 increased gradually with the development of embryos. By contrast, CBX5 maintained a high expression level during oocyte maturation, and decreased rapidly after fertilization and remained low expression in preimplantation embryos. In addition, CBX5 was increased in the *Rnf114*$^{m-z+}$ two-cell embryos (Fig. S5C,D), indicating the potential influence of abnormally accumulated CBX5 protein on embryo development. To examine this hypothesis, we microinjected the *in vitro*-transcribed mRNA of *Cbx5* into WT zygotes and evaluated the consequences of overexpressing CBX5 on embryos. CBX3 overexpression was also monitored at the same time (Fig. 6A). Firstly, western blot analysis confirmed the efficient overexpression

Development (2021) 148, dev199426. doi:10.1242/dev.199426

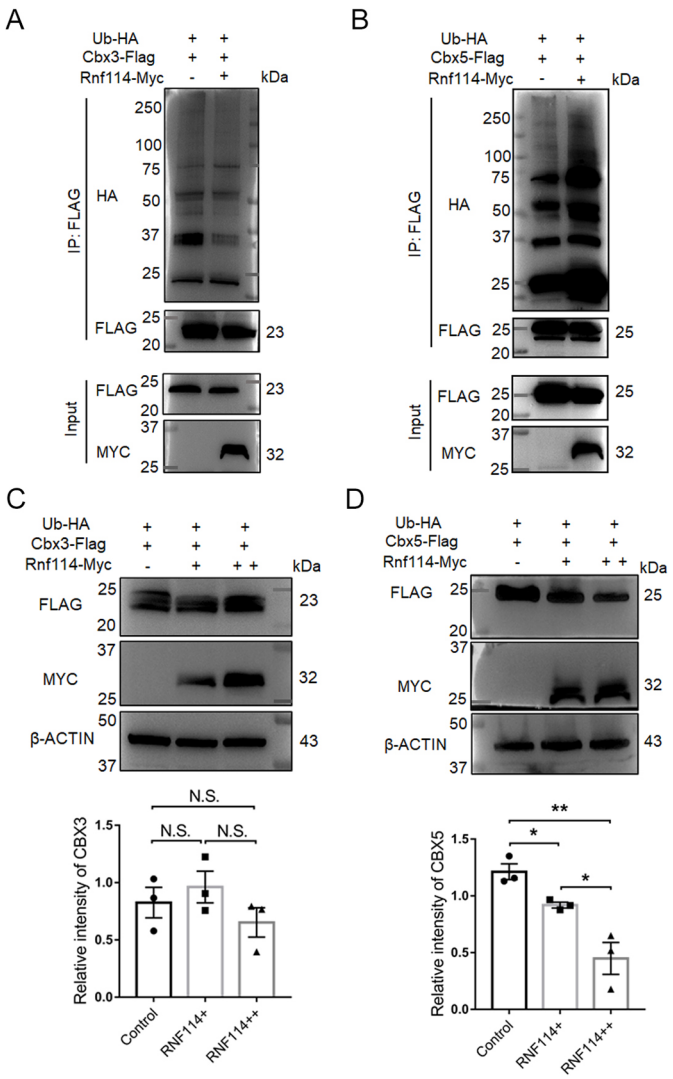

Fig. 5. RNF114 mediates the ubiquitylation and degradation of CBX5, but not CBX3. (A,B) Representative immunoblots showing the ubiquitylation levels of CBX3 (A) and CBX5 (B) with or without RNF114 overexpression. 293T cells expressing *Cbx5*-Flag or *Cbx3*-Flag and HA-*Ub* were cotransfected with or without the Rnf114-Myc plasmid. Cellular lysate was immunoprecipitated using anti-Flag affinity beads, followed by western blot. Cellular lysate was used as the input. *n*=3, independent replicates. (C,D) Representative western blot showing the protein levels of CBX3 (C) and CBX5 (D) with different expression levels of RNF114. The expression of corresponding CBX proteins was measured. β-Actin was used as the loading control. *n*=3, independent replicates. Data are mean±s.e.m. N.S., no significance. **P*<0.05, ***P*<0.01 compared with the control group (unpaired two-tailed *t*-test).

of CBX proteins (Fig. 6B,C). Compared with the control embryos which were injected with H_2O, the development of zygotes microinjected with *Cbx5* mRNA was severely impaired from the four-cell to the blastocyst stage. However, zygotes injected with *Cbx3* mRNA showed few changes (Fig. 6D,E). EU incorporation indicated that the transcription level of embryos expressing exogenous CBX5 generally decreased at the two-cell stage; nevertheless, embryos with CBX3 overexpression were not affected (Fig. 6F,G). Furthermore, the level of genes from the major ZGA cluster according to the DBTMEE database was reduced significantly in two-cell embryos injected with *Cbx5* mRNA but slightly changed in embryos injected with *Cbx3* (Fig. 6H). As a whole, the abnormal accumulation of CBX5 protein in oocytes was sustained in the *Rnf114* mutant embryos. CBX5 overexpression hindered embryonic development, mainly disturbing the activation of major ZGA, which was consistent with the results of maternal RNF114 deletion.

Abnormal increases in TAB1 also contributes to the failure of major ZGA

In a previous study, the mechanism of RNF114-mediated ubiquitylation and degradation of TAB1, promoting embryonic development, was discovered (Yang et al., 2017). In this model, western blot analysis revealed that the level of TAB1 also increased in the *Rnf114*$^{m-z+}$ two-cell embryos (Fig. S6A,B). To illustrate the relationship between the elevated TAB1 protein and major ZGA, TAB1 was overexpressed by *Tab1* mRNA microinjection into WT zygotes. EU incorporation in the two-cell embryos derived from treated zygotes was significantly decreased (Fig. S6C,D). The major ZGA genes were also detected with different degrees of decline in TAB1-overexpressed two-cell embryos (Fig. S6E).

To further confirm that the cumulative CBX5 and TAB1 gave rise to embryonic development arrest and major ZGA abnormality in maternal RNF114 depleted embryos, we injected *Cbx5* and *Tab1* siRNA into the *Rnf114*$^{m-z+}$ zygotes to rescue the mutant embryos, respectively (Fig. 7A). More mutant embryos injected with *Cbx5* and *Tab1* siRNA developed to the four-cell stage, compared with the control embryos. Although these embryos gradually blocked at subsequent stages, a few embryos could reach to the blastocyst stage in the rescued group (Fig. 7B,C). Also, some major ZGA genes were increased significantly in the treated two-cell embryos (Fig. 7D). This phenomenon suggested that the mechanism of embryonic retardation caused by maternal RNF114 deletion was complicated and maternal RNF114 participated in the regulation of multiple pathways during embryogenesis by degrading substrate proteins, thus activating major ZGA and promoting early embryonic development.

DISCUSSION

In mammals, major ZGA is considered to be the starting point for embryonic characteristic acquisition, as oocyte identity is nearly erased via the degradation of maternal factors (Svoboda, 2018). Major ZGA is primarily regulated by maternal factors that accumulate and store in mature oocytes during the period of genomic transcriptional silencing (Li et al., 2010). The expression pattern of RNF114 in oocytes and pre-implantation embryos indicates its similarity to the maternal protein. Previously, knockdown of *Rnf114* by injection of siRNA into zygotes resulted in the abnormal development of mouse embryos (Yang et al., 2017). However, this strategy could not prove the maternal role for RNF114 on mouse embryos. Therefore, we generated *Rnf114*-mutant mice through gene editing techniques. Although the deletion did not cause a frameshift mutation, the transcription and protein levels of RNF114 were both significantly reduced. The destruction of the RING domain in RNF114 may result in its degradation because the key domains are important to protein stability (Heessen et al., 2005; Liu et al., 2017). The instability of mutant mRNA was unexpected, although the degradation of mutant mRNA had been previously demonstrated in some gene-edited animals (Oo et al., 2020; Xu et al., 2020). The female mice were completely sterile after *Rnf114* editing. Further experiments revealed that embryos fertilized by *Rnf114*-null oocytes and WT sperm did not survive past the two-cell embryonic stage. These results confirmed the maternal influence exerted through RNF114 during embryogenesis.

Development (2021) 148, dev199426. doi:10.1242/dev.199426

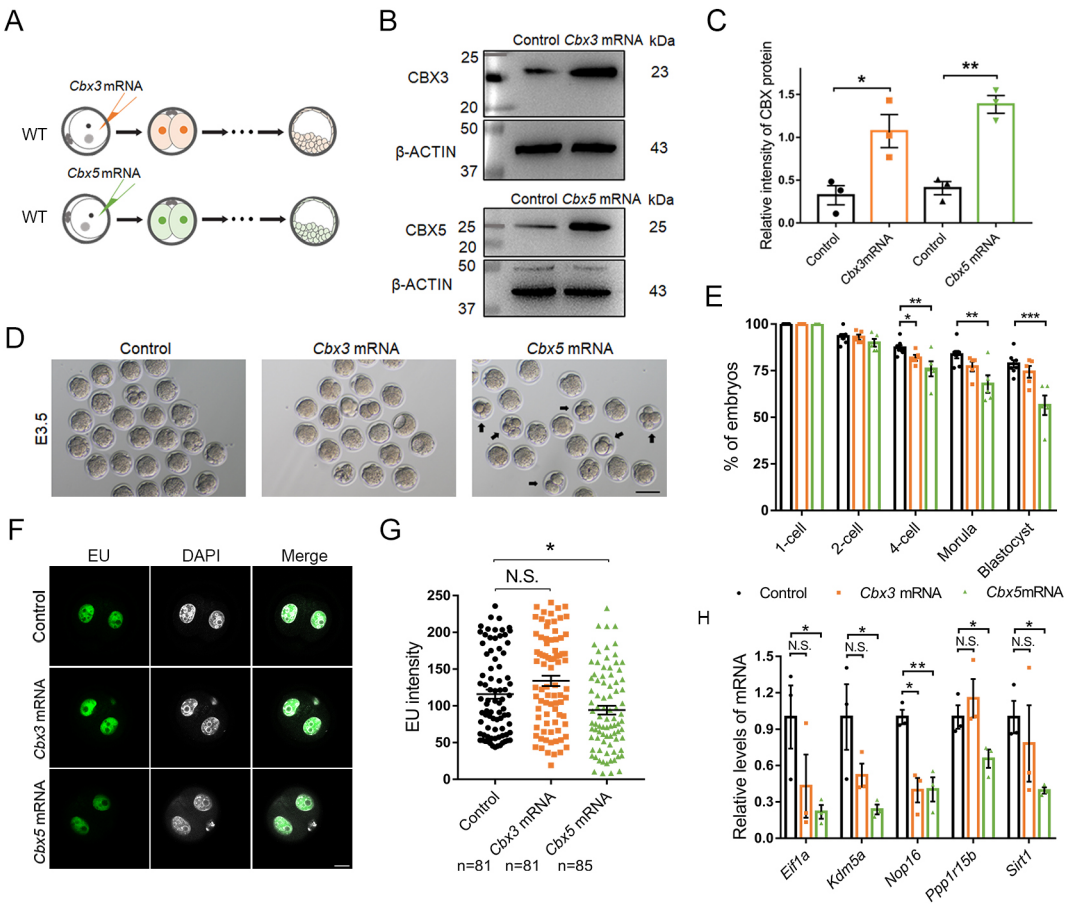

Fig. 6. Embryos overexpressing CBX5 have decreased major ZGA. (A) Overview of *Cbx3* and *Cbx5* mRNA overexpression. (B) Immunoblot showing the levels of CBX3 and CBX5 in two-cell embryos after microinjecting mRNA. β-Actin was used as the loading control. *n*=3, independent replicates. (C) Quantification of the grey scale from B. (D) Representative differential interference contrast images of the control and overexpressed embryos at E3.5. The arrows point to the embryos with developmental arrest. Scale bar: 100 µm. (E) Percentage of embryos derived from overexpressed Cbx3 and Cbx5 zygotes to the preimplantation embryo stages. *n*=5, total of 202-448 embryos/group. (F) The intensity of EU incorporation in the control and CBX3- and CBX5-overexpressing two-cell embryos. Scale bar: 20 µm. (G) Quantification of EU staining from F. Error bars represent s.e.m. (H) Quantitative RT-PCR results showing the expression level of the major ZGA genes in the control and overexpressed two-cell embryos. *n*=3, independent replicates. Data are mean±s.e.m. N.S., no significance. **P*<0.05, ***P*<0.01, ****P*<0.001 compared with the control group (unpaired two-tailed *t*-test).

Transcription assays showed the failure of major ZGA in the absence of maternal RNF114. Dysregulated maternal RNA metabolism appeared in the mutant two-cell embryo transcriptome at the same time, with many maternal RNAs overstocking. We also identified DEGs at the MII and one-cell stages. As shown in Fig. 3C, there were 138 DEGs in the MII oocytes and 13 DEGs in the one-cell embryos. We found that these DEGs were mainly concentrated in a range with FPKM<10 (86.76%), which is the standard range indicating low expression (Benfeitas et al., 2019), and these genes largely disappeared from the DEGs in the subsequent developmental stage. These phenomena illustrated the instability of the DEGs at low abundance. Therefore, although the number of DEGs at MII stage was more than 100, the mutant group was unable to be distinguished completely from the control by PC1 or PC2 in the PCA analysis. In addition, GO analysis was performed on the upregulated and downregulated genes in the MII oocytes, but no GO term was enriched (FDR<0.05). The detection of minor ZGA by EU incorporation and Pol II Ser-2p/5p staining demonstrated a normal transcription level at the one-cell stage. In general, this study highlights the essential role of maternal RNF114 in initiating major ZGA during embryonic development.

To investigate the mechanism of RNF114 blocking embryonic development and major ZGA, proteomic analysis of MII oocytes was performed to determine the substrates of RNF114. Although relevant experiments confirmed that the absence of RNF114 did not affect oocyte quality and fertilization, the proteomic analysis results suggested that RNF114 deletion might disrupt oocyte proteometabolism. We found that only two genes in the transcriptome and proteome overlapped at the MII stage, *Rnf114* and *Kat14*, both of which were downregulated. It has been reported that *Kat14* knockout affects histone acetylation, leading to cell cycle blockade in the G2/M phase and mouse embryo arrest at E8.5 (Guelman et al., 2009; Suganuma et al., 2008). We observed two enriched clusters of differentially expressed proteins associated with ‘cytomembrane’ and ‘chromatin’ in an interaction network analysis. LYZ1, the most significantly changed protein in the ‘cytomembrane’ cluster, is a marker for Paneth cells, a type of intestinal epithelial cell (Bel et al., 2017). LYZ1 is secreted into the extracellular region to dissolve bacteria and stabilize the intestinal environment (Yu et al., 2020). Some proteins in the Annexin family were also identified, including ANXA1, ANXA2, ANXA3 and ANXA11. These proteins are mainly reported to be related to embryo implantation and post-implantation development (Hebeda et al., 2018, 2020; Kultima et al.,

Development (2021) 148, dev199426. doi:10.1242/dev.199426

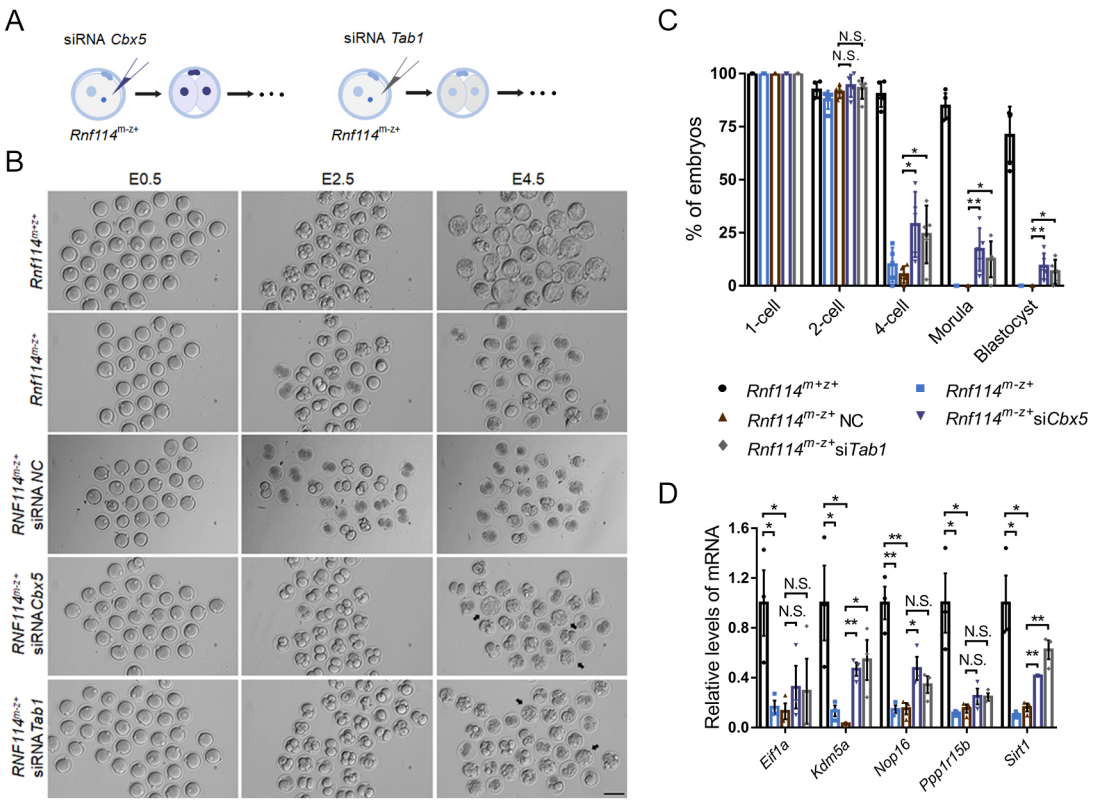

Fig. 7. Knockdown of *Cbx5* and *Tab1* partially rescues the phenotypes in maternal RNF114-depleted embryos. (A) Overview of *Cbx5* and *Tab1* knockdown in maternal RNF114-depleted embryos. (B) Representative differential interference contrast images of the treated embryos at E0.5, E2.5 and E4.5. The arrows point to the embryos that developed into the blastocysts. Scale bar: 100 µm. (C) Percentage of embryos derived from control and treated zygotes to the preimplantation embryo stages. *n*=5, total of 114-192 embryos/group. (D) Quantitative RT-PCR results showing the expression level of the major ZGA genes in the control and knockdown two-cell embryos. *n*=3, independent replicates. Data are mean±s.e.m. N.S., no significance. **P*<0.05, ***P*<0.01 compared with the control group (unpaired two-tailed *t*-test).

2004; Meadows and Cleaver, 2015; Wang and Shao, 2020). To date, no evidence supports their relationship to the MZT process. On the other hand, the structure and state of chromatin change dramatically during embryogenesis (Fu et al., 2020). Some histone subunits were disturbed in the RNF114-null oocytes, with abnormal accumulation of HIST1H1E (H1F4) and H2AFV (H2AZ2) and decreased HIST1H1T (H1F6) content. Histone 1 variants may have a compensatory effect, whereas HIST1H1T is a specific histone in male germ cells (Nguyen et al., 2014; Sarg et al., 2009). H2AFV, a histone 2 variant, plays a role in regulating the formation of heterochromatin and gene transcription in *Drosophila* (Giaimo et al., 2019; Swaminathan et al., 2005). Whether the changes in several histone variants have an effect on embryo development needs to be further investigated in the future. We focused on CBX3 and CBX5 in the 'chromatin' cluster, the GO annotations of which hinted at a potential opposite force on mouse embryonic development. First, the relationship between RNF114 and the CBX proteins was verified. Some studies reported that FBXW10 or RNF123 ubiquitin ligase promoted the proteasomal degradation of CBX5 but not CBX3 in HeLa cells with mislocalization or reduced expression of lamins (Chaturvedi et al., 2012; Chaturvedi and Parnaik, 2010). We also found that RNF114 ubiquitylated and degraded the CBX5 protein but not CBX3 in 293T cells. In follow-up work, the regulation of CBX5 by RNF114 needs to be verified in oocytes. CBX5 expression has been reported to decrease rapidly after fertilization, and its level is not re-elevated until post-implantation (Wongtawan et al., 2011), findings verified by our experiments. In addition, CBX5 was independently increased in mutant two-cell embryos. The abnormal accumulation of CBX5 in mutant embryos may have adverse effects on early embryos. WT zygotes injected with *Cbx5* mRNA were blocked from the four-cell stage, and major ZGA was abnormally decreased. The effect of upregulated CBX5 in maternal RNF114-deficient embryos was confirmed by the exogenous expression of CBX5 in WT embryos.

As a member of the heterochromatin protein family, CBX5 plays an important role in many biological events, such as DNA replication, transcription and histone modification (Bártová et al., 2017; Larson et al., 2017; Ryan and Tremethick, 2018). The CBX5 protein contains two conserved domains, the amino-terminal region known as the chromodomain (CD), which interacts with methylated lysine 9 residues on histone 3 (H3K9me), leading to the assembly of transcription inhibition complexes (Eisert and Waters, 2011; Fischle et al., 2005; Stewart et al., 2005). Therefore, CBX5 may function as a gene silencer to suppress the activation of major ZGA, and the underlying mechanisms need to be further explored. The other domain of CBX5 is the carboxy-terminal chromoshadow domain (CSD), which is a platform for binding certain proteins, including CBX proteins (Eissenberg and Elgin, 2014; Richart et al., 2012). This means that the accumulation of CBX3 in oocytes may be indirectly caused by the formation of CBX3-CBX5 heterodimers.

Notably, the phenotype of embryos after maternal *Rnf114* deletion was more severely abnormal than that of embryos with exogenous CBX5 overexpression. This suggested that there might be other mechanisms interfering with embryonic development. Considering previous work, we explored the change in TAB1 expression in

Development (2021) 148, dev199426. doi:10.1242/dev.199426

maternal RNF114-deletion embryos. Although TAB1 expression was gently increased in *Rnf114*$^{m-z+}$ two-cell embryos, it was not detected in the protein profile. The reason may be insufficient detection sensitivity of the mass spectrometry (MS) analyses. Furthermore, TAB1 is ubiquitously expressed in murine post-implantation embryos (Komatsu et al., 2002), whereas the expression of TAB1 is relatively low and thus difficult to detect in oocytes. The transcriptional level in two-cell embryos overexpressing exogenous TAB1 was decreased. In addition, knocking down *Cbx5* or *Tab1* partially rescued the phenotypes acquired after the deletion of maternal RNF114 in mutant embryos. Although both TAB1 and CBX5 are substrates for RNF114 and their overexpression affects major ZGA and embryonic development, no association between TAB1 and CBX5 has been reported. Whether there is a link between the two proteins remains to be further explored.

In conclusion, RNF114 is highly expressed and exerts the effect of a ubiquitin E3 ligase in mouse oocytes under physiological conditions. It mediates the degradation of substrates such as CBX5 and TAB1 for subsequent major ZGA. Loss of RNF114 leads to the accumulation of its substrates, which block the normal process of the MZT and fails to initiate major ZGA in mouse embryos. It is tempting to hypothesize that RNF114, as a crucial maternal regulator, might participate in the cross-talk required for adequate clearance of maternal proteins and activation of the early zygotic genome.

MATERIALS AND METHODS

The generation of Rnf114 knockout mice

We used CRISPR Cas9 to construct gene-edited mice. The T7 promoter and the guiding sequence were added to the sgRNA by PCR amplification. The primers for sgRNA are listed in Table S6. B6D2F1 (C57BL/6 × DBA2, RRID: IMSR_JAX: 100006) female mice and ICR mice were used as embryo donors and foster mothers, respectively. Superovulated female B6D2F1 mice (6-8 weeks old) were mated with B6D2F1 males, and the fertilized embryos were collected from the oviducts. Cas9 mRNA (100 ng/µl) and sgRNA (20 ng/µl) were injected into the cytoplasm of fertilized eggs with well-recognized pronuclei in M2 medium (Sigma-Aldrich, M7167). The injected zygotes were cultured in KSOM (modified simplex-optimized medium, Millipore, MR-020P-D) at 37°C under 5% CO_2 in air, and 15-25 blastocysts were transferred into the uterus of pseudopregnant ICR females. See Table S6 for genotyping primers. Mouse experiments were carried out according to and with the approval of the Institutional Animal Care and Use Committee of Nanjing Medical University, China. All husbandry and procedures involving the mice were carried out according to the Guide for the Care and Use of Laboratory Animals (National Research Council, 2011).

Fertility assessment and ovarian histology analysis

For fertility assessment, *Rnf114*$^{+/-}$ and *Rnf114*$^{-/-}$ females were mated with WT males at a ratio of 2:1 over 6 months. Ovaries from 8-week-old female mice were fixed in 4% paraformaldehyde overnight at 4°C, embedded in paraffin, serially sectioned at 5 µm using a microtome (RM2235, Leica), and stained with haematoxylin and eosin (H&E). The total number of follicles at various developmental stages was counted using a double-blind method. The morphology of the follicles and the follicle-containing method have been previously described (Hu et al., 2020).

Superovulation, *in vitro* fertilization and culture embryos

Female mice at 6-8 weeks of age were intraperitoneally injected with 5 IU pregnant mare serum gonadotropin (PMSG), and 5 IU human chorionic gonadotropin (HCG) was injected 46-48 h later. The cumulus-oocyte complexes were harvested from the ampullae of oviducts with M2 medium at 13-14 h post-HCG. The number of oocytes was counted after cumulus removal by digestion with hyaluronidase (Sigma-Aldrich, H3506). For *in vitro* fertilization, cumulus-oocyte complexes were collected with human tubular fluid (HTF; Irvine Scientific, 90125) as described above. The sperm from wild mouse epididymis capacitated in HTF medium. The sperm were added to the HTF, containing cumulus-oocyte complexes, which were then cultured for 4-6 h in a humidified atmosphere of 5% CO_2 at 37°C and then transferred to KSOM for further cultivation. Embryos were manipulated at the indicated time points after insemination: one-cell, 10-12 hours post insemination (hpi); two-cell, 30-32 hpi, as previously described (Aoki et al., 1997).

Real-time PCR

Total RNA was isolated from oocytes using the RNeasy Mini kit (Qiagen, 74034), followed by reverse transcription using a PrimeScript RT Reagent Kit (Takara, RR036A). Quantitative real-time PCR was performed using Power SYBR Green PCR Master Mix (Vazyme, Q711-02) to test the expression of the corresponding genes. We used 18S rRNA as internal control and the relative changes in gene expression were calculated by $2_T^{-\Delta\Delta C}$ method. Specific primers are listed in Table S6.

Immunofluorescence staining

Oocytes and embryos were fixed in 4% paraformaldehyde (Sigma-Aldrich, P6148) in PBS for 30 min at room temperature, permeabilized for 15 min in 0.5% Triton X-100 in PBS, blocked with 5% bovine serum albumin (BSA) for 1 h at room temperature, and incubated in primary antibodies overnight at 4°C. Next, the samples were washed three times with washing buffer (PBS with 0.1% Triton X-100), incubated in secondary antibodies for 1 h at room temperature, and stained with Hoechst 33342 (Invitrogen, H21492) for 5 min at room temperature. The images were obtained using a confocal laser scanning microscope (LSM 800, Carl Zeiss), and fluorescence intensity was quantified using ZEN 2012 Bule Edition (Carl Zeiss). The antibodies used are listed in Table S7.

Transcription assays

Embryos were cultured in KSOM with 1 mM EU for 2 h and fixed in 4% paraformaldehyde in PBS for 30 min at room temperature. EU incorporation into the RNA was detected using the Click-iT RNA Alexa Fluor 594 Imaging Kit (Invitrogen, C10330) according to the manufacturer's instructions. Fluorescence was detected using confocal laser scanning microscopy (LSM 800, Carl Zeiss).

Western blot

One hundred embryos and mouse ovaries were lysed in RIPA lysis buffer (CWBio, CW2333) containing protease inhibitor cocktail (CWBio, CW2200) and phosphatase inhibitor cocktail (CWBio, CW2383). For the mouse ovaries and 293T cells, the lysate was sonicated five times for 3 s each time. Samples were incubated on ice for 30 min, centrifuged at 16,000 ***g*** for 30 min, mixed with protein loading buffer (FDBio, FD002) and boiled for 5 min. Western blotting was carried out using standard procedures as previously described (Zhang et al., 2018). The lysate was separated by 4-20% SDS-PAGE and transferred onto PVDF membranes (Millipore, IPVH00010). Afterwards, the membranes were blocked in 5% skimmed milk for 2 h at room temperature and then incubated overnight in primary antibody at 4°C. After three washes in 200 mM Tris-HCl, 3 M NaCl, 0.1% Tween 20, pH 7.2-7.5 (TBST), the membranes were incubated with the corresponding secondary antibody for 2 h at room temperature and detected using a horseradish peroxidase (HRP)-enhanced chemiluminescence kit (FDBio, FD8020). Densitometry of the western blot bands was performed using ImageJ software. The indicated antibodies are listed in Table S7.

Construction of plasmids

For the construction of expression vectors for the ubiquitylation assay, mouse *Rnf114* was subcloned into pCMV6-Entry, which has a Myc tag. In addition, *Cbx3-Flag* and *Cbx5-Flag* were cloned into the pCMV6-Entry vector. Ubiquitin cDNA with an HA tag was cloned into the pcDNA3.1+ vector. For *in vitro* transcription, mouse *Cbx3*, *Cbx5* and *Tab1* were cloned into the pCS2+ vector.

In vitro transcription

The expression vectors were linearized by KpnI and purified using a QIAquick PCR purification kit (Qiagen, 28104). The linearized DNAs were

Development (2021) 148, dev199426. doi:10.1242/dev.199426

transcribed *in vitro* by the Sp6 message transcription kit (Invitrogen, AM1340). The capped mRNAs were purified using the RNeasy cleanup kit (Qiagen, 74204) and dissolved in nuclease-free water up to 1000 ng/µl.

Microinjection of zygotes

For microinjection, mouse zygotes were harvested in M2 medium at 6 hpi. Approximately 5-10 pl samples were microinjected into each zygote. Then, the microinjected zygotes were cultured in prewarmed KSOM at 37°C with 5% CO_2. The sequences of siRNA are listed in Table S6.

Ubiquitylation assay

HEK293T cells were grown in DMEM (Gibco, 11995065) supplemented with 10% foetal bovine serum and 1% penicillin streptomycin solution at 37°C in a 5% CO_2 in air atmosphere. After transfection with various mixtures of plasmids as indicated, the 293T cells were treated with MG132 (5 µM) for 4 h to inhibit proteasome activity. The cells were lysed in RIPA lysis buffer (Beyotime, P0013K) supplemented with a 1 mM protease inhibitor cocktail (Bimake, B14001), sonicated five times for 3 s each time and rocked gently at 4°C for 30 min. After centrifugation for 60 min at 18,000 ***g*** at 4°C, the supernatant was immunoprecipitated by anti-Flag affinity beads (Smart Life Sciences, SA042001) and eluted with acid elution (0.1 M glycine-HCl, pH 3.0). Then, samples were analysed with western blot. Ubiquitylation analysis was carried out using tag antibodies (Table S7). The total lysate was used as the input. For the experiment of substrate degradation, the 293T cells, which were transfected with various mixtures of plasmids, were cultivated at 37°C in a 5% CO_2 in air atmosphere without MG132 treatment. Then, samples were lysed in RIPA lysis buffer and analysed with western blot.

RNA sequencing and analysis

Oocytes and embryos were collected at the time point as described in Table S1. The RNA-seq libraries for the harvested samples were generated based on Smart-seq2 (Picelli et al., 2014). Sequence libraries were constructed using the KAPA HyperPlus Prep Kit (KK8514) according to the manufacturer's instructions. All libraries were sequenced on an Illumina HiSeq2500 with paired-end 150-bp sequencing. The RNA-seq experiments are deposited in NCBI GEO under accession number GSE164532. The read quality was controlled using fastqc and trim_galore. Clean reads were aligned to the mouse genome mm10 using HISAT2 with default parameters. The read counts were quantified using featureCounts. Differential expression testing was performed using the R package DESeq2. Genes with adjusted P-value<0.05 and a fold change>2 were marked as DEGs. GO analysis was performed using DAVID. Major ZGA and maternal gene clusters were obtained from DBTMEE database. The significant P-values of $\log_2$ (upregulated genes/downregulated genes) in control group versus mutant group were determined using Fisher's exact test. Heatmaps were prepared using the R package heatmap. Other plots were prepared using the R package ggplot2.

Mass spectrometry

Oocytes were harvested from the *Rnf114*$^{+/-}$ and *Rnf114*$^{-/-}$ mice. The proteins were reduced, and trypsin was digested and desalted as described previously (Wang et al., 2015). For TMT labelling, purified peptides were reconstituted in 200 mM triethylammonium bicarbonate (TEAB) and labelled using TMT 6-plex (Thermo Fisher Scientific, 90066) according to the manufacturer's instructions (Fan et al., 2020). All labelled peptide samples were combined, purified using an OASIS HLB Vac cartridge and lyophilized. Then, the mixed TMT-labelled peptides were separated by high-pH reversed-phase (HP-RP) fractionation technology based on the ACQUITY UPLC M-class system (Waters) with a BEH C18 column (300 µm×150 mm, 1.7 µm; Waters), and 30 fractions were collected and lyophilized as previously described (Li et al., 2020).

For liquid chromatograph mass spectrometer (LC-MS) analyses, peptides were resuspended in 0.1% formic acid and analysed using an LTQ Orbitrap Fusion Lumos mass spectrometer (Thermo Fisher Scientific) coupled to an Easy-nLC 1200 (Thermo Fisher Scientific). The trap column (75 µm×2 cm, Acclaim® PepMap100 C18 column, 3 µm, 100 Å; DIONEX) effluent was transferred to a reverse-phase microcapillary column (75 µm×25 cm, Acclaim® PepMap RSLC C18 column, 2 µm, 100 Å; DIONEX). The Orbitrap Fusion Lumos mass spectrometer was operated in the data-dependent mode. A full survey scan was obtained for the m/z range of 350-1500, and the resolution of HCD MS/MS was 15,000. Raw files were searched against the mouse protein sequences obtained from the Universal Protein Resource (UniProt) database by MaxQuant software (version 1.6.2.10) (Tyanova et al., 2016). Carbamidomethyl (C) on cysteine was fixed modifications with TMT reagent adducts on lysine and peptide amino termini as fixed modifications for the TMT data. Variable modifications included oxidation (M) and acetylation (protein N-term). False discovery rate (FDR) cut-offs were set to 0.01 for proteins, peptides and sites.

Differential proteins were determined using the unpaired two-tailed Student's t-test. A P-value less than 0.05 and fold change of *Rnf114*$^{-/-}$/*Rnf114*$^{+/-}$ of more than 1.2 or less than 0.833 were considered significant, as shown by the protein-protein interaction networks using the STRING and Cytoscape software. Enrichment analysis of gene ontology, including biological process, cellular component and molecular function terms, was carried out using the clusterProfiler R package (Yu et al., 2012). The proteomics data have been deposited in the ProteomeXchange Consortium via the proteomics identifications (PRIDE) database (Identifier PXD023458).

Statistical analysis

Comparisons between two groups were analysed using unpaired two-tailed t-tests in GraphPad Prism 7.0. The statistical significance was as follows: N.S., not significant, P>0.05; *P<0.05; **P<0.01; ***P<0.001.

Competing interests

The authors declare no competing or financial interests.

Author contributions

Methodology: Y.G., Y.H., X.G.; Validation: R.H.; Formal analysis: H.S., L.Y., S.C., X.G.; Investigation: S.Z., L.L., C.Z., M.L., Y.C., C.W., Q.L., R.H.; Resources: C.L., W.L., R.H.; Data curation: H.S., L.Y., Y.H., R.H.; Writing - original draft: S.Z., R.H.; Supervision: W.L., X.G., R.H.; Funding acquisition: R.H.

Funding

This work was supported by the National Key Research and Development Program of China (2018YFC1004002), National Natural Science Foundation of China (31671566, 32070838), Postgraduate Education Reform Project of Jiangsu Province (KYCX19_1144) and Open Fund of State Key Laboratory of Reproductive Medicine of Nanjing Medical University (SKLRM-201806).

Data availability

RNA-seq data are deposited in GEO under accession number GSE164532. The proteomics data have been deposited in the ProteomeXchange Consortium under accession number PXD023458.

Peer review history

The peer review history is available online at https://journals.biologists.com/dev/article-lookup/doi/10.1242/dev.199426

References

Abe, K.-I., Funaya, S., Tsukioka, D., Kawamura, M., Suzuki, Y., Suzuki, M. G., Schultz, R. M. and Aoki, F. (2018). Minor zygotic gene activation is essential for mouse preimplantation development. *Proc. Natl. Acad. Sci. USA* **115**, E6780-E6788. doi:10.1073/pnas.1804309115

Aoki, F., Worrad, D. M. and Schultz, R. M. (1997). Regulation of transcriptional activity during the first and second cell cycles in the preimplantation mouse embryo. *Dev. Biol.* **181**, 296-307. doi:10.1006/dbio.1996.8466

Bártová, E., Malyšková, B., Komůrková, D., Legartová, S., Suchánková, J., Krejčí, J. and Kozubek, S. (2017). Function of heterochromatin protein 1 during DNA repair. *Protoplasma* **254**, 1233-1240. doi:10.1007/s00709-017-1090-3

Bel, S., Pendse, M., Wang, Y., Li, Y., Ruhn, K. A., Hassell, B., Leal, T., Winter, S. E., Xavier, R. J. and Hooper, L. V. (2017). Paneth cells secrete lysozyme via secretory autophagy during bacterial infection of the intestine. *Science (New York, N.Y.)* **357**, 1047-1052. doi:10.1126/science.aal4677

Benfeitas, R., Bidkhori, G., Mukhopadhyay, B., Klevstig, M., Arif, M., Zhang, C., Lee, S., Cinar, R., Nielsen, J., Uhlen, M. et al. (2019). Characterization of heterogeneous redox responses in hepatocellular carcinoma patients using network analysis. *EBioMedicine* **40**, 471-487. doi:10.1016/j.ebiom.2018.12.057

Chaturvedi, P. and Parnaik, V. K. (2010). Lamin A rod domain mutants target heterochromatin protein 1alpha and beta for proteasomal degradation by activation of F-box protein, FBXW10. *PLoS ONE* **5**, e10620. doi:10.1371/journal.pone.0010620

Chaturvedi, P., Khanna, R. and Parnaik, V. K. (2012). Ubiquitin ligase RNF123 mediates degradation of heterochromatin protein 1α and β in lamin A/C knock-down cells. *PLoS ONE* **7**, e47558. doi:10.1371/journal.pone.0047558

Egloff, S. and Murphy, S. (2008). Cracking the RNA polymerase II CTD code. *Trends Genet.* **24**, 280-288. doi:10.1016/j.tig.2008.03.008

Eisert, R. J. and Waters, M. L. (2011). Tuning HP1α chromodomain selectivity for di- and trimethyllysine. *Chembiochem* **12**, 2786-2790. doi:10.1002/cbic.201100555

Eissenberg, J. C. and Elgin, S. C. R. (2014). HP1a: a structural chromosomal protein regulating transcription. *Trends Genet.* **30**, 103-110. doi:10.1016/j.tig.2014.01.002

Esencan, E., Kallen, A., Zhang, M. and Seli, E. (2019). Translational activation of maternally derived mRNAs in oocytes and early embryos and the role of embryonic poly(A) binding protein (EPAB). *Biol. Reprod.* **100**, 1147-1157. doi:10.1093/biolre/ioz034

Fan, Y., Cheng, Y., Li, Y., Chen, B., Wang, Z., Wei, T., Zhang, H., Guo, Y., Wang, Q., Wei, Y. et al. (2020). Phosphoproteomic analysis of neonatal regenerative myocardium revealed important roles of checkpoint kinase 1 via activating mammalian target of Rapamycin C1/Ribosomal Protein S6 Kinase b-1 Pathway. *Circulation* **141**, 1554-1569. doi:10.1161/CIRCULATIONAHA.119.040747

Fischle, W., Tseng, B. S., Dormann, H. L., Ueberheide, B. M., Garcia, B. A., Shabanowitz, J., Hunt, D. F., Funabiki, H. and Allis, C. D. (2005). Regulation of HP1-chromatin binding by histone H3 methylation and phosphorylation. *Nature* **438**, 1116-1122. doi:10.1038/nature04219

Fu, X., Zhang, C. and Zhang, Y. (2020). Epigenetic regulation of mouse preimplantation embryo development. *Curr. Opin. Genet. Dev.* **64**, 13-20. doi:10.1016/j.gde.2020.05.015

Giaimo, B. D., Ferrante, F., Herchenröther, A., Hake, S. B. and Borggrefe, T. (2019). The histone variant H2A.Z in gene regulation. *Epigenet. Chromatin* **12**, 37. doi:10.1186/s13072-019-0274-9

Giannini, A. L., Gao, Y. and Bijlmakers, M.-J. (2008). T-cell regulator RNF125/TRAC-1 belongs to a novel family of ubiquitin ligases with zinc fingers and a ubiquitin-binding domain. *Biochem. J.* **410**, 101-111. doi:10.1042/BJ20070995

Guelman, S., Kozuka, K., Mao, Y., Pham, V., Solloway, M. J., Wang, J., Wu, J., Lill, J. R. and Zha, J. (2009). The double-histone-acetyltransferase complex ATAC is essential for mammalian development. *Mol. Cell. Biol.* **29**, 1176-1188. doi:10.1128/MCB.01599-08

Han, J., Kim, Y.-L., Lee, K.-W., Her, N.-G., Ha, T.-K., Yoon, S., Jeong, S.-I., Lee, J.-H., Kang, M.-J., Lee, M.-G. et al. (2013). ZNF313 is a novel cell cycle activator with an E3 ligase activity inhibiting cellular senescence by destabilizing p21(WAF1.). *Cell Death Differ.* **20**, 1055-1067. doi:10.1038/cdd.2013.33

Hebeda, C. B., Machado, I. D., Reif-Silva, I., Moreli, J. B., Oliani, S. M., Nadkarni, S., Perretti, M., Bevilacqua, E. and Farsky, S. H. P. (2018). Endogenous annexin A1 (AnxA1) modulates early-phase gestation and offspring sex-ratio skewing. *J. Cell. Physiol.* **233**, 6591-6603. doi:10.1002/jcp.26258

Hebeda, C. B., Sandri, S., Benis, C. M., Paula-Silva, M., Loiola, R. A., Reutelingsperger, C., Perretti, M. and Farsky, S. H. P. (2020). Annexin A1/Formyl peptide receptor pathway controls uterine receptivity to the blastocyst. *Cells* **9**:1188. doi:10.3390/cells9051188

Heessen, S., Masucci, M. G. and Dantuma, N. P. (2005). The UBA2 domain functions as an intrinsic stabilization signal that protects Rad23 from proteasomal degradation. *Mol. Cell* **18**, 225-235. doi:10.1016/j.molcel.2005.03.015

Hu, Y., Ouyang, Z., Sui, X., Qi, M., Li, M., He, Y., Cao, Y., Cao, Q., Lu, Q., Zhou, S. et al. (2020). Oocyte competence is maintained by m(6)A methyltransferase KIAA1429-mediated RNA metabolism during mouse follicular development. *Cell Death Differ.* **27**, 2468-2483. doi:10.1038/s41418-020-0516-1

Huang, Y., Kim, J. K., Do, D. V., Lee, C., Penfold, C. A., Zylicz, J. J., Marioni, J. C., Hackett, J. A. and Surani, M. A. (2017). Stella modulates transcriptional and endogenous retrovirus programs during maternal-to-zygotic transition. *eLife* **6**, e22345. doi:10.7554/eLife.22345

Jao, C. Y. and Salic, A. (2008). Exploring RNA transcription and turnover in vivo by using click chemistry. *Proc. Natl. Acad. Sci. USA* **105**, 15779-15784. doi:10.1073/pnas.0808480105

Kim, K.-H. and Lee, K.-A. (2014). Maternal effect genes: Findings and effects on mouse embryo development. *Clin. Exp. Reprod. Med.* **41**, 47-61. doi:10.5653/cerm.2014.41.2.47

Ko, M. S. H. (2016). Zygotic genome activation revisited: looking through the expression and function of Zscan4. *Curr. Top. Dev. Biol.* **120**, 103-124. doi:10.1016/bs.ctdb.2016.04.004

Komatsu, Y., Shibuya, H., Takeda, N., Ninomiya-Tsuji, J., Yasui, T., Miyado, K., Sekimoto, T., Ueno, N., Matsumoto, K. and Yamada, G. (2002). Targeted disruption of the Tab1 gene causes embryonic lethality and defects in cardiovascular and lung morphogenesis. *Mech. Dev.* **119**, 239-249. doi:10.1016/S0925-4773(02)00391-X

Kultima, K., Nyström, A.-M., Scholz, B., Gustafson, A.-L., Dencker, L. and Stigson, M. (2004). Valproic acid teratogenicity: a toxicogenomics approach. *Environ. Health Perspect.* **112**, 1225-1235. doi:10.1289/txg.7034

Kumar, A. and Kono, H. (2020). Heterochromatin protein 1 (HP1): interactions with itself and chromatin components. *Biophys. Rev.* **12**, 387-400. doi:10.1007/s12551-020-00663-y

Larson, A. G., Elnatan, D., Keenen, M. M., Trnka, M. J., Johnston, J. B., Burlingame, A. L., Agard, D. A., Redding, S. and Narlikar, G. J. (2017). Liquid droplet formation by HP1α suggests a role for phase separation in heterochromatin. *Nature* **547**, 236-240. doi:10.1038/nature22822

Li, L., Zheng, P. and Dean, J. (2010). Maternal control of early mouse development. *Development* **137**, 859-870. doi:10.1242/dev.039487

Li, L., Zhu, S., Shu, W., Guo, Y., Guan, Y., Zeng, J., Wang, H., Han, L., Zhang, J., Liu, X. et al. (2020). Characterization of metabolic patterns in mouse oocytes during meiotic maturation. *Mol. Cell* **80**, 525-540.e529. doi:10.1016/j.molcel.2020.09.022

Lin, B., Ke, Q., Li, H., Pheifer, N. S., Velliquette, D. C. and Leaman, D. W. (2017). Negative regulation of the RLH signaling by the E3 ubiquitin ligase RNF114. *Cytokine* **99**, 186-193. doi:10.1016/j.cyto.2017.05.002

Lin, B., Ke, Q., Leaman, D. W., Goel, V. and Agarwal, A. (2018). Regulation of RANKL-induced osteoclastogenesis by RING finger protein RNF114. *J. Orthop. Res.* **36**, 159-166. doi:10.1002/jor.23654

Liu, F., Qin, Y., Yu, S., Soares, D. C., Yang, L., Weng, J., Li, C., Gao, M., Lu, Z., Hu, X. et al. (2017). Pathogenic mutations in retinitis pigmentosa 2 predominantly result in loss of RP2 protein stability in humans and zebrafish. *J. Biol. Chem.* **292**, 6225-6239. doi:10.1074/jbc.M116.760314

Liu, H.-B., Muhammad, T., Guo, Y., Li, M.-J., Sha, Q.-Q., Zhang, C.-X., Liu, H., Zhao, S.-G., Zhao, H., Zhang, H. et al. (2019). RNA-binding protein IGF2BP2/IMP2 is a critical maternal activator in early zygotic genome activation. *Adv. Sci.* **6**, 1900295. doi:10.1002/advs.201900295

Lykke-Andersen, K., Gilchrist, M. J., Grabarek, J. B., Das, P., Miska, E. and Zernicka-Goetz, M. (2008). Maternal Argonaute 2 is essential for early mouse development at the maternal-zygotic transition. *Mol. Biol. Cell* **19**, 4383-4392. doi:10.1091/mbc.e08-02-0219

Maison, C. and Almouzni, G. (2004). HP1 and the dynamics of heterochromatin maintenance. *Nat. Rev. Mol. Cell Biol.* **5**, 296-305. doi:10.1038/nrm1355

Meadows, S. M. and Cleaver, O. (2015). Annexin A3 regulates early blood vessel formation. *PLoS ONE* **10**, e0132580. doi:10.1371/journal.pone.0132580

Nagaraj, R., Sharpley, M. S., Chi, F., Braas, D., Zhou, Y., Kim, R., Clark, A. T. and Banerjee, U. (2017). Nuclear localization of mitochondrial TCA cycle enzymes as a critical step in mammalian zygotic genome activation. *Cell* **168**, 210-223.e211. doi:10.1016/j.cell.2016.12.026

National Research Council (2011). *Guide for the Care and Use of Laboratory Animals*, 8th edn. Washington, DC: The National Academies Press.

Nguyen, G. D., Gokhan, S., Molero, A. E., Yang, S.-M., Kim, B.-J., Skoultchi, A. I. and Mehler, M. F. (2014). The role of H1 linker histone subtypes in preserving the fidelity of elaboration of mesendodermal and neuroectodermal lineages during embryonic development. *PLoS ONE* **9**, e96858. doi:10.1371/journal.pone.0096858

Oo, Z. M., Adlat, S., Sah, R. K., Myint, M. Z. Z., Hayel, F., Chen, Y., Htoo, H., Bah, F. B., Bahadar, N., Chan, M. K. et al. (2020). Brain transcriptome study through CRISPR/Cas9 mediated mouse Dip2c gene knock-out. *Gene* **758**, 144975. doi:10.1016/j.gene.2020.144975

Park, S.-J., Shirahige, K., Ohsugi, M. and Nakai, K. (2015). DBTMEE: a database of transcriptome in mouse early embryos. *Nucleic Acids Res.* **43**, D771-D776. doi:10.1093/nar/gku1001

Picelli, S., Faridani, O. R., Björklund, A. K., Winberg, G., Sagasser, S. and Sandberg, R. (2014). Full-length RNA-seq from single cells using Smart-seq2. *Nat. Protoc.* **9**, 171-181. doi:10.1038/nprot.2014.006

Richart, A. N., Brunner, C. I. W., Stott, K., Murzina, N. V. and Thomas, J. O. (2012). Characterization of chromoshadow domain-mediated binding of heterochromatin protein 1α (HP1α) to histone H3. *J. Biol. Chem.* **287**, 18730-18737. doi:10.1074/jbc.M111.337204

Ryan, D. P. and Tremethick, D. J. (2018). The interplay between H2A.Z and H3K9 methylation in regulating HP1α binding to linker histone-containing chromatin. *Nucleic Acids Res.* **46**, 9353-9366. doi:10.1093/nar/gky632

Sarg, B., Chwatal, S., Talasz, H. and Lindner, H. H. (2009). Testis-specific linker histone H1t is multiply phosphorylated during spermatogenesis. Identification of phosphorylation sites. *J. Biol. Chem.* **284**, 3610-3618. doi:10.1074/jbc.M805925200

Sha, Q.-Q., Zhang, J. and Fan, H.-Y. (2019). A story of birth and death: mRNA translation and clearance at the onset of maternal-to-zygotic transition in mammals†. *Biol. Reprod.* **101**, 579-590. doi:10.1093/biolre/ioz012

Stewart, M. D., Li, J. and Wong, J. (2005). Relationship between histone H3 lysine 9 methylation, transcription repression, and heterochromatin protein 1 recruitment. *Mol. Cell. Biol.* **25**, 2525-2538. doi:10.1128/MCB.25.7.2525-2538.2005

Suganuma, T., Gutiérrez, J. L., Li, B., Florens, L., Swanson, S. K., Washburn, M. P., Abmayr, S. M. and Workman, J. L. (2008). ATAC is a double histone

acetyltransferase complex that stimulates nucleosome sliding. *Nat. Struct. Mol. Biol.* **15**, 364-372. doi:10.1038/nsmb.1397

Svoboda, P. (2018). Mammalian zygotic genome activation. *Semin. Cell Dev. Biol.* **84**, 118-126. doi:10.1016/j.semcdb.2017.12.006

Swaminathan, J., Baxter, E. M. and Corces, V. G. (2005). The role of histone H2Av variant replacement and histone H4 acetylation in the establishment of Drosophila heterochromatin. *Genes Dev.* **19**, 65-76. doi:10.1101/gad.1259105

Tong, Z.-B., Gold, L., Pfeifer, K. E., Dorward, H., Lee, E., Bondy, C. A., Dean, J. and Nelson, L. M. (2000). Mater, a maternal effect gene required for early embryonic development in mice. *Nat. Genet.* **26**, 267-268. doi:10.1038/81547

Toralova, T., Kinterova, V., Chmelikova, E. and Kanka, J. (2020). The neglected part of early embryonic development: maternal protein degradation. *Cellular and molecular life sciences : CMLS* **77**, 3177-3194. doi:10.1007/s00018-020-03482-2

Tyanova, S., Temu, T. and Cox, J. (2016). The MaxQuant computational platform for mass spectrometry-based shotgun proteomics. *Nat. Protoc.* **11**, 2301-2319. doi:10.1038/nprot.2016.136

Vastenhouw, N. L., Cao, W. X. and Lipshitz, H. D. (2019). The maternal-to-zygotic transition revisited. *Development (Cambridge, England)* **146**, dev161471. doi:10.1242/dev.161471

Wang, B. and Shao, Y. (2020). Annexin A2 acts as an adherent molecule under the regulation of steroids during embryo implantation. *Mol. Hum. Reprod.* **26**, 825-836. doi:10.1093/molehr/gaaa065

Wang, S., Kou, Z., Jing, Z., Zhang, Y., Guo, X., Dong, M., Wilmut, I. and Gao, S. (2010). Proteome of mouse oocytes at different developmental stages. *Proc. Natl. Acad. Sci. USA* **107**, 17639-17644. doi:10.1073/pnas.1013185107

Wang, J., Qi, L., Huang, S., Zhou, T., Guo, Y., Wang, G., Guo, X., Zhou, Z. and Sha, J. (2015). Quantitative phosphoproteomics analysis reveals a key role of insulin growth factor 1 receptor (IGF1R) tyrosine kinase in human sperm capacitation. *Mol. Cell. Proteomics* **14**, 1104-1112. doi:10.1074/mcp.M114.045468

Wongtawan, T., Taylor, J. E., Lawson, K. A., Wilmut, I. and Pennings, S. (2011). Histone H4K20me3 and HP1α are late heterochromatin markers in development, but present in undifferentiated embryonic stem cells. *J. Cell Sci.* **124**, 1878-1890. doi:10.1242/jcs.080721

Wu, D. and Dean, J. (2016). BTG4, a maternal mRNA cleaner. *J. Mol. Cell Biol.* **8**, 369-370. doi:10.1093/jmcb/mjw031

Xu, K., Han, C. X., Zhou, H., Ding, J. M., Xu, Z., Yang, L. Y., He, C., Akinyemi, F., Zheng, Y. M., Qin, C. et al. (2020). Effective MSTN Gene Knockout by AdV-Delivered CRISPR/Cas9 in Postnatal Chick Leg Muscle. *Int. J. Mol. Sci.* **21**, 2584. doi:10.3390/ijms21072584

Yang, P., Lu, Y., Li, M., Zhang, K., Li, C., Chen, H., Tao, D., Zhang, S. and Ma, Y. (2014). Identification of RNF114 as a novel positive regulatory protein for T cell activation. *Immunobiology* **219**, 432-439. doi:10.1016/j.imbio.2014.02.002

Yang, Y., Zhou, C., Wang, Y., Liu, W., Liu, C., Wang, L., Liu, Y., Shang, Y., Li, M., Zhou, S. et al. (2017). The E3 ubiquitin ligase RNF114 and TAB1 degradation are required for maternal-to-zygotic transition. *EMBO Rep.* **18**, 205-216. doi:10.15252/embr.201642573

Yu, G., Wang, L.-G., Han, Y. and He, Q.-Y. (2012). clusterProfiler: an R package for comparing biological themes among gene clusters. *Omics* **16**, 284-287. doi:10.1089/omi.2011.0118

Yu, S., Balasubramanian, I., Laubitz, D., Tong, K., Bandyopadhyay, S., Lin, X., Flores, J., Singh, R., Liu, Y., Macazana, C. et al. (2020). Paneth cell-derived lysozyme defines the composition of mucolytic microbiota and the inflammatory tone of the intestine. *Immunity* **53**, 398-416.e398. doi:10.1016/j.immuni.2020.07.010

Zhang, P., Ni, X., Guo, Y., Guo, X., Wang, Y., Zhou, Z., Huo, R. and Sha, J. (2009). Proteomic-based identification of maternal proteins in mature mouse oocytes. *BMC Genomics* **10**, 348. doi:10.1186/1471-2164-10-348

Zhang, Y. L., Zhao, L. W., Zhang, J., Le, R., Ji, S. Y., Chen, C., Gao, Y., Li, D., Gao, S. and Fan, H. Y. (2018). DCAF13 promotes pluripotency by negatively regulating SUV39H1 stability during early embryonic development. *EMBO J.* **37**, e98981. doi:10.15252/embj.201898981

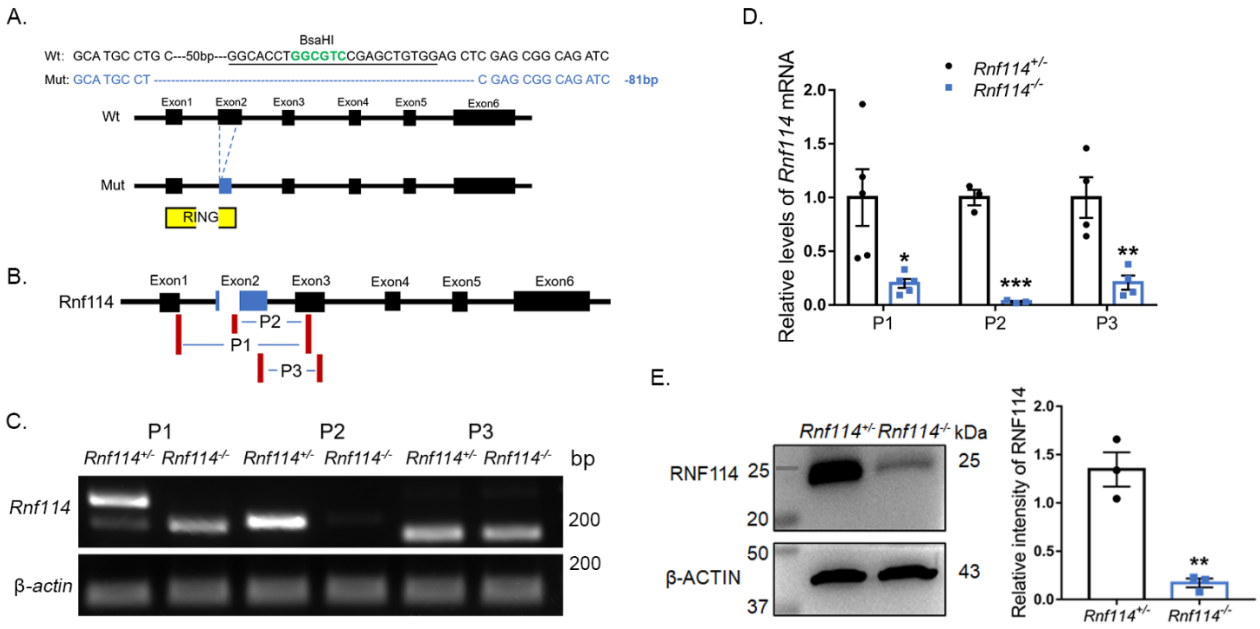

Figure S1.

(A, B) Diagrams showing the deletion of sequences from the mouse *Rnf114* gene locus, the destruction of the RNF114 protein domain (A) and the location of primers (B) designed to detect the knockout efficiency. (C) Representative images of *Rnf114* mRNA levels primed by P1, P2, and P3 in *Rnf114*$^{+/-}$ and *Rnf114*$^{-/-}$ metaphase II (MII) oocytes. β-actin was the loading control for the integrity of the RNA samples. N = 3 independent replicates. (D) Quantitative RT-PCR results showing *Rnf114* mRNA levels primed by P1, P2, and P3 in *Rnf114*$^{+/-}$ and *Rnf114*$^{-/-}$ MII oocytes. N = 3-5 independent replicates. (E) Immunoblot showing the RNF114 protein levels in *Rnf114*$^{+/-}$ and *Rnf114*$^{-/-}$ ovaries. Corresponding gray scale were measured. β-Actin was the loading control. N = 3, independent replicates. All graphs are presented as the means ± SEM. $^{**}P < 0.05$, $^{**}P < 0.01$, $^{***}P < 0.001$ compared to the control group in the unpaired two-tailed t-test.

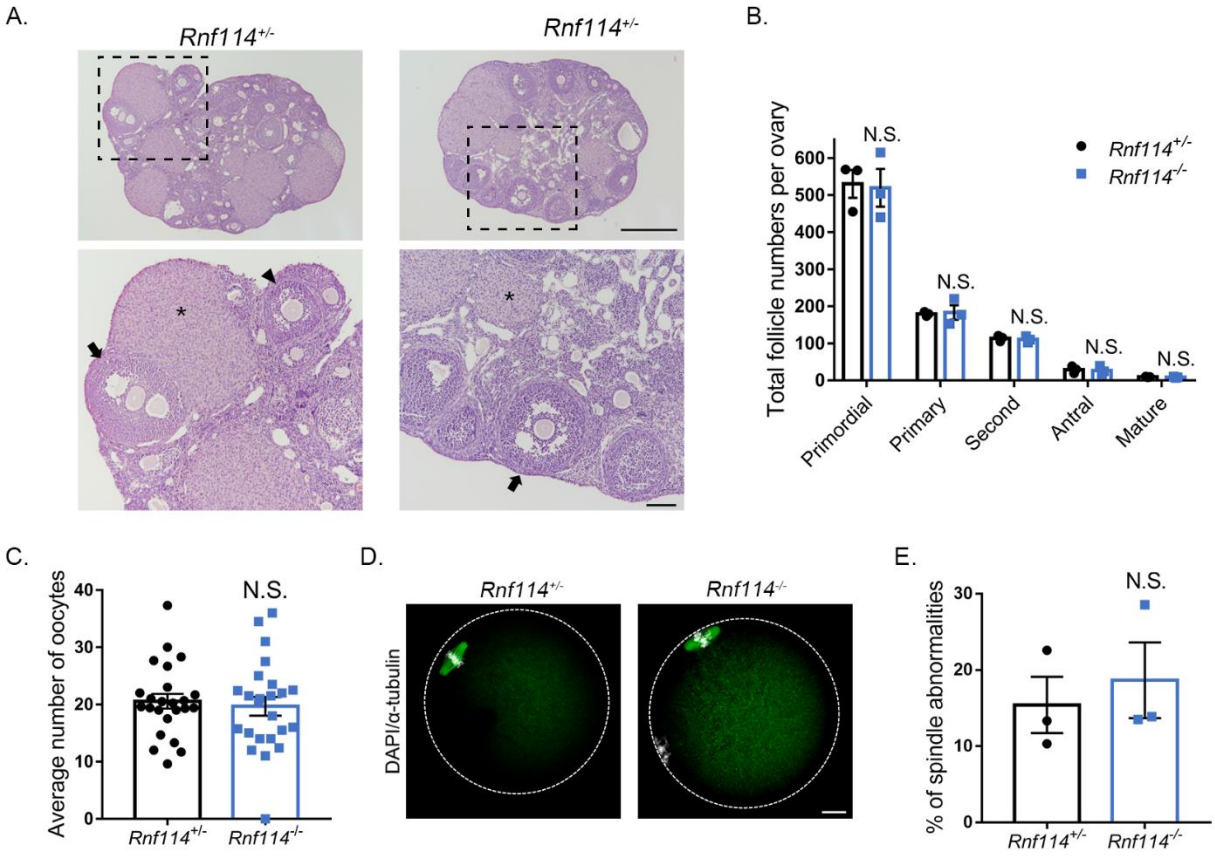

Figure S2.

(A) H- and E-stained images showing the ovarian histology of *Rnf114*$^{+/-}$ and *Rnf114*$^{-/-}$ females. The black dotted lines represent the enlarged areas. Antral follicles (arrowheads), secondary follicles (arrows) follicles, and corpora lutea (*) are indicated. Scale bar = 500 μm in the whole picture and scale bar = 100 μm in the greater zoom. (B) The average of follicle count at each stage in the control and mutant mice. N = 3, independent replicates. (C) Average number of MII oocytes from *Rnf114*$^{+/-}$ and *Rnf114*$^{-/-}$ females after superovulation. N = 24, total of 61-82 mice/group. (D) Microscopic images showing spindles in the *Rnf114*$^{+/-}$ and *Rnf114*$^{-/-}$ MII oocytes. Dashed lines indicate oocyte outlines. Scale bar = 20 μm. (E) Spindle abnormalities in the *Rnf114*$^{+/-}$ and *Rnf114*$^{-/-}$ MII oocytes. N = 3, total of 90-94 oocytes for each group. The above graphs are presented as the means ± SEM. N.S. = no significance in the unpaired two-tailed t-test.

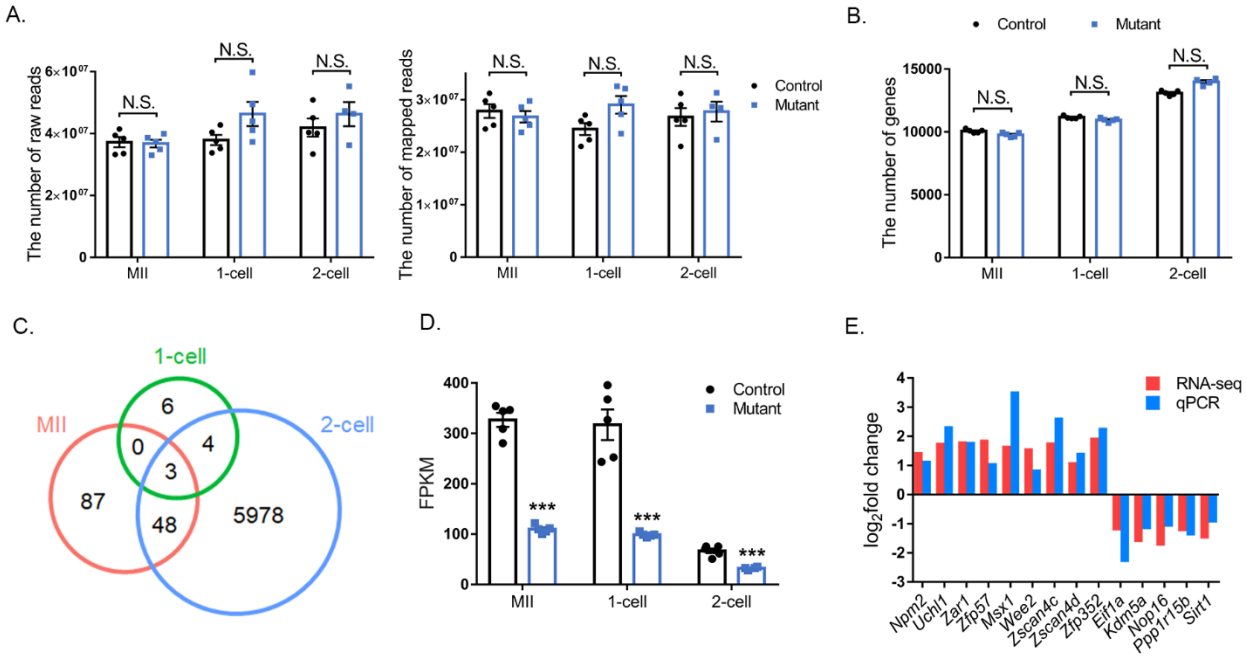

Figure S3.

(A) The average number of raw and mapped reads in control and mutant group. N = 4-5, independent replicates. (B)The average number of genes detected in control and mutant group, with FPKM >1 as the gene expression threshold. N = 4-5, independent replicates. (C) A Venn diagram illustrating the overlap of DEGs in MII oocytes and 1-cell and 2-cell embryos. (D) FPKM statistics for the RNF114 gene in the control and mutant groups at different time points. N = 4-5, independent replicates. Data are presented as the means ± SEM. N.S. = no significance, ***$P < 0.001$ in the unpaired two-tailed t-test. (E) The log_2-fold change of representative DEGs and corresponding qRT-PCR verification results. This qRT-PCR was performed on independent samples with 3 independent replicates.

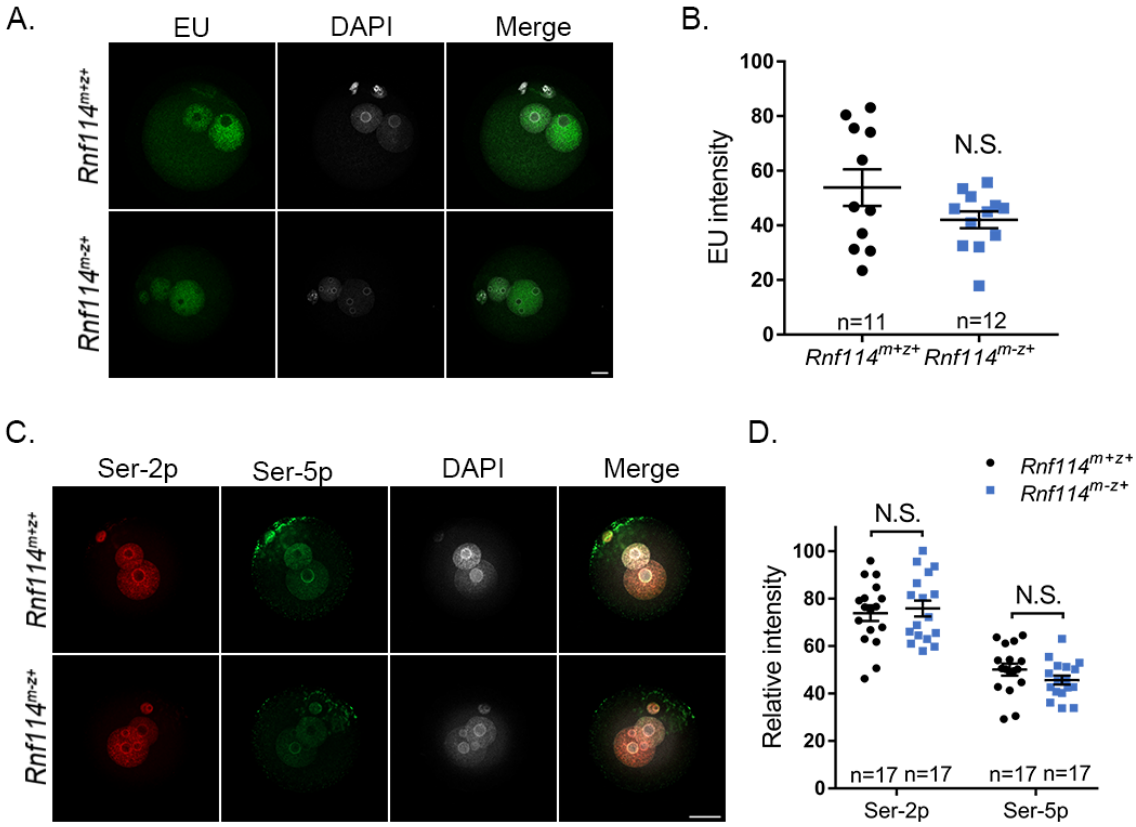

Figure S4.

(A, B) EU staining (A) and quantification of EU staining (B) in *Rnf114*$^{m+z+}$ and *Rnf114*$^{m-z+}$ 1-cell embryos. (C) Phosphorylation levels of serine moieties at positions 2 and 5 of Pol II for *Rnf114*$^{m+z+}$ and *Rnf114*$^{m-z+}$ 1-cell embryos. (D) Quantification of Ser-2p and Ser-5p staining. All error bars represent SEM. N.S. = no significance in the unpaired two-tailed t-test. All scale bar = 20 μm.

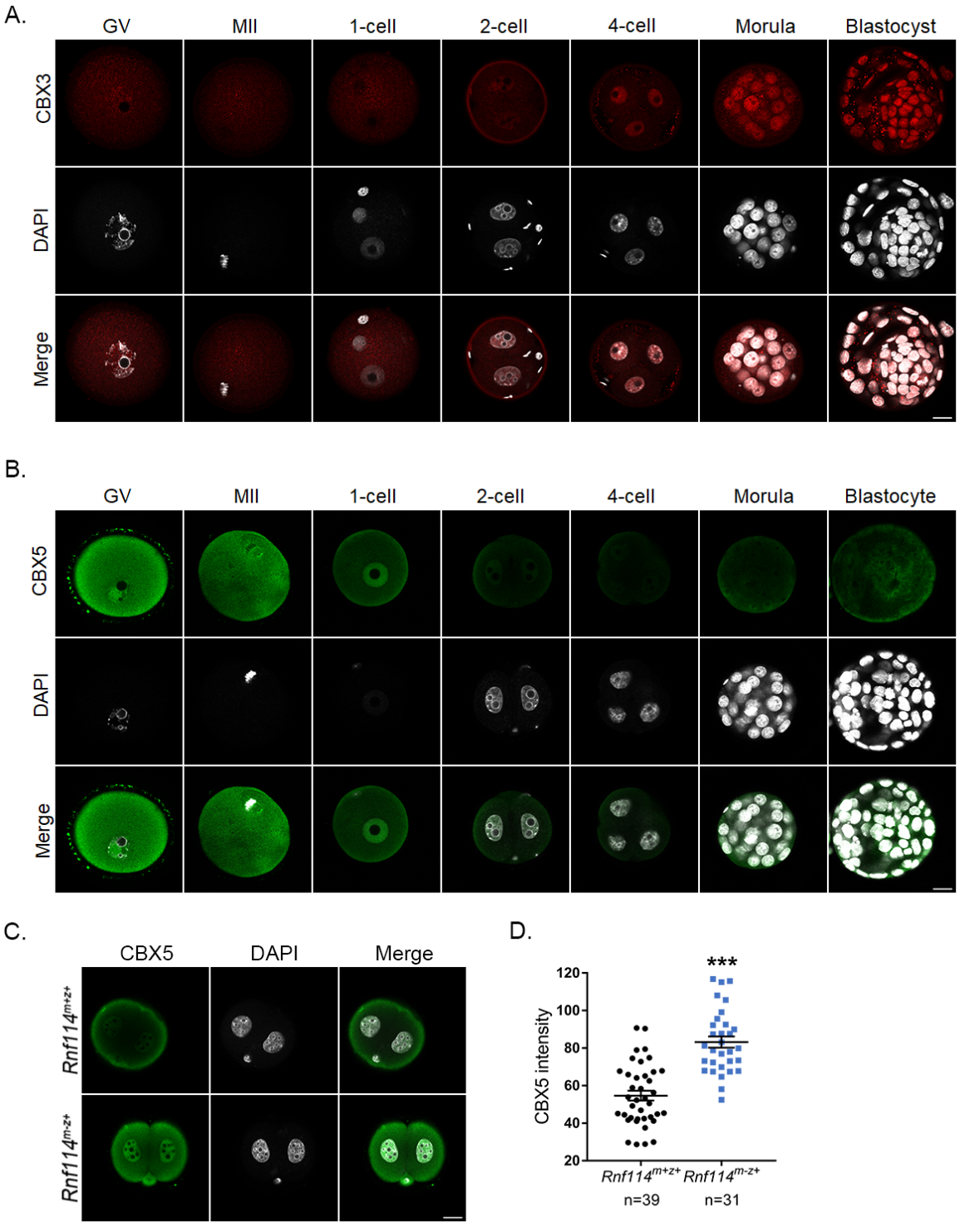

Figure S5.

(A, B) The expression of CBX3 (A) and CBX5 (B) in oocytes and preimplantation embryos. (C) Representative immunofluorescence images of CBX5 in the *Rnf114*$^{m+z+}$ and *Rnf114*$^{m-z+}$ 2-cell embryos. (D) Quantification of CBX5 staining in the *Rnf114*$^{m+z+}$ and *Rnf114*$^{m-z+}$ 2-cell embryos. Error bars represent SEM. ***P < 0.001 in the unpaired two-tailed t-test. All 90 scale bar = 20 μm.

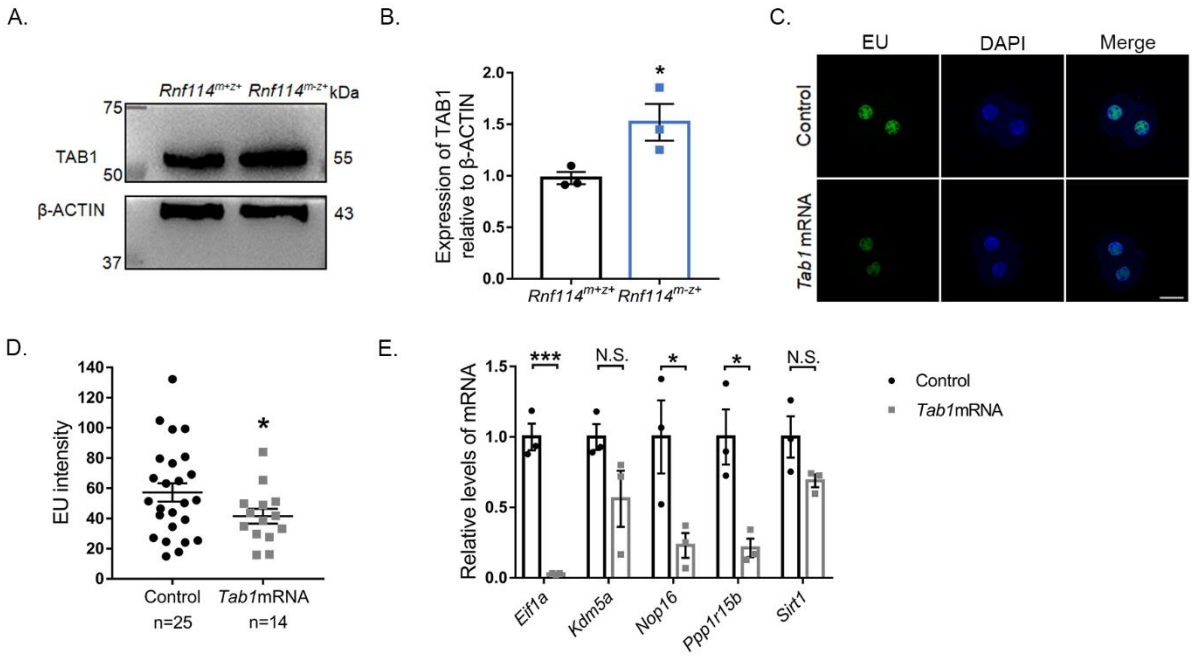

Figure S6.

(A) Representative western blot showing the levels of TAB1 in *Rnf114*$^{m+z+}$ and *Rnf114*$^{m-z+}$ 2-cell embryos. β-Actin was used as a loading control. (B) Quantitative analysis of the TAB1 protein from western blot. N = 3, independent replicates. Data are presented as the means ± SEM. (C) Representative images of EU staining after overexpressing *Tab1* in the WT 2-cell embryos. Scale bars = 20 μm. (D) Quantification of EU staining in WT 2-cell embryos with TAB1 overexpression. Error bars represent SEM. (E) Quantitative RT-PCR results showing the expression level of major ZGA genes in the WT 2-cell embryos with overexpressed TAB1 protein. N = 3, independent replicates. All graphs are presented as the means ± SEM. N.S. = no significance, **P* < 0.05, ****P* < 0.001 in the unpaired two-tailed t-test.

Table S1. Sample details for RNA sequencing

Click here to download Table S1

Table S2. All DEGs between the control and mutant groups via RNA sequencing analysis at the MII oocyte, 1-cell and 2-cell embryo stages (adjusted P-value < 0.05).

Click here to download Table S2

Table S3. Enriched GO terms for DEGs in the *Rnf114*$^{m-z+}$ 2-cell embryos compared with those in *Rnf114*$^{m+z+}$ (FDR < 0.05)

Click here to download Table S3

Table S4. Differential expression of proteins in the *Rnf114*$^{-/-}$ oocytes identified by mass spectrometry (P-value < 0.05)

Click here to download Table S4

Table S5. Top twenty significant GO catalogues of differentially expressed proteins in the *Rnf114*$^{-/-}$ oocytes

Click here to download Table S5

Table S6. List of primer sequences and the sequences of siRNA in this study

Click here to download Table S6

Table S7. Detailed information on the antibodies used for western blot and immunofluorescence staining

Click here to download Table S7